



HAL
open science

Timing, duration and role of magmatism in wide rift systems: Insights from the Jiaodong Peninsula (China, East Asia)

Nicolas Charles, Romain Augier, Charles Gumiaux, Patrick Monié, Yan Chen,
Michel Faure, Rixiang Zhu

► **To cite this version:**

Nicolas Charles, Romain Augier, Charles Gumiaux, Patrick Monié, Yan Chen, et al.. Timing, duration and role of magmatism in wide rift systems: Insights from the Jiaodong Peninsula (China, East Asia). *Gondwana Research*, 2013, 24, pp.412-428. <10.1016/j.jgr.2012.10.011>. <insu-00752551>

HAL Id: insu-00752551

<https://insu.hal.science/insu-00752551v1>

Submitted on 19 Nov 2012

HAL is a multi-disciplinary open access archive for the deposit and dissemination of scientific research documents, whether they are published or not. The documents may come from teaching and research institutions in France or abroad, or from public or private research centers.

L'archive ouverte pluridisciplinaire **HAL**, est destinée au dépôt et à la diffusion de documents scientifiques de niveau recherche, publiés ou non, émanant des établissements d'enseignement et de recherche français ou étrangers, des laboratoires publics ou privés.



HAL Authorization

Timing, duration and role of magmatism in wide rift systems: Insights from the Jiaodong Peninsula (China, East Asia)

Nicolas Charles^{1,2,3,6*}, Romain Augier^{1,2,3}, Charles Gumiaux^{1,2,3}, Patrick Monié⁴, Yan Chen^{1,2,3},
Michel Faure^{1,2,3}, Rixiang Zhu⁵.

1: Université d'Orléans, ISTO, UMR7327 45071, Orléans, France.

2: CNRS/INSU, ISTO, UMR7327, 45071 Orléans, France.

3: BRGM, ISTO, UMR7327, BP36009, 45060 Orléans, France.

4: Géosciences Montpellier, UMR5243, Université Montpellier 2-CNRS, 34095 Montpellier, France.

5: Institute of Geology and Geophysics, Chinese Academy of Sciences, Beijing 100029, China.

6: Now at: Bureau de Recherches Géologiques et Minières (BRGM), 3 avenue Claude Guillemin, BP36009, 45060 Orléans, France.

*Corresponding author: n.charles@brgm.fr

Abstract

In East Asia, widespread extensional sedimentary basins together with the close association of Metamorphic Core Complexes and magmatism are prominent features of the large-scale wide rift system developed during late Mesozoic times. This region thus appears as a proper place to study continental extension as well as questions about the link between continental extension and magmatism. This paper primarily provides pioneer exhumation time-constraints on the Linglong MCC (Jiaodong Peninsula) including cooling and deformation ages. MCC cooling at mid-crustal levels occurred at ca. 143 Ma. Besides, last ductile deformation occurred at ca. 134 Ma while final exhumation stages, under brittle

conditions, occurred as late as ca. 128 Ma. Continuous crustal stretching were then recorded by the emplacement of a synkinematic pluton in the upper crust at ca. 128 Ma that cooled fast below an intracrustal shear zone crossing the ductile-brittle transition at ca. 123 Ma. The ca. 120-118 Ma age cluster is ascribed to the fast cooling of undeformed plutons marking the end of extension that lasted, in the area, over a minimum period of ca. 30 My. Combining other MCC exhumation constraints and the onset of subsidence in the sedimentary basins, total duration of late Mesozoic extension in East Asia could be estimated at ca. 60 My, related with a rather long process for extension from 160 to at least 100 Ma. East Asian continental extension is heterogeneously distributed in space and time as revealed by fundamental differences between two end-member classes of migmatite-cored MCC already described in other wide rift systems. Extension seems to have first favoured partial melting which subsequently, in turn, maintained continental extension.

Key-words: continental extension, magmatism, MCCs, $^{40}\text{Ar}/^{39}\text{Ar}$, late Mesozoic, East Asia.

1. Introduction

Continental extension is one of the most remarkable geodynamic processes affecting the lithosphere and attracts considerable attention of the geosciences community (e.g. England, 1983; Buck, 1991; Corti et al., 2003). Basically, continental lithosphere can be stretched following two principal modes of extension: (1) narrow rift and (2) wide rift systems (Buck, 1991; Brun, 1999; Corti et al., 2003). Narrow rifts display rather localised deformation within the continental lithosphere and correspond to continental rifts that may lead to continent break-up in more mature stages (Brun, 1999). Conversely, wide rifts concern very large strained areas (~1000 km wide) and comprise, among other structures, metamorphic

core complexes (MCCs; Brun, 1999). Areas such as the Basin & Range (North America) and Aegean (Mediterranean Sea) regions, illustrate well the wide rift mode of extension (Buck, 1991; Corti et al., 2003, see references therein). Since the past three decades, field work (e.g. Davis and Coney, 1979; Crittenden et al., 1980; Lister et al., 1984; Lister and Davis, 1989; Gautier et al., 1993; Jolivet and Brun, 2010), as well as analogue and numerical modelling (e.g. Brun et al., 1994; Tirel et al., 2006, 2008) highly improved our knowledge and comprehension on the modes of extension in such domains. In particular, theories on the geodynamic causes generating wide rift systems, including subducting lithospheric slab movements, have been well developed (e.g. Rosenbaum et al., 2008; Jolivet et al., 2009a; Jolivet and Brun, 2010). Yet, in spite of the increasing amount of both geological data and mechanical models, two major points dealing with extension mechanisms are still discussed: (1) the timing and duration of deformation processes, and more particularly of MCCs development (e.g. Gautier et al., 1999; Sullivan and Snoke, 2007) and (2) the genetic link between regional-scale extension and magmatism in a broad sense (e.g. Crittenden et al., 1980; Reynolds and Rehrig, 1980; Coney and Harms, 1984; Lynch and Morgan, 1987; Lister and Davis, 1989; Tomassi et al., 1994; Gautier et al., 1999; Corti et al., 2003; Tirel et al., 2008; Péron-Pinvidic et al., 2009; Rey et al., 2009a, b).

East Asia has been marked by large-scale continental extension during late Mesozoic (e.g. Menzies et al., 1993; Ren et al., 2002; Meng, 2003; Lin and Wang, 2006; Zhai et al., 2007; Charles et al., 2011a, 2012) and thus constitutes a third example of wide rift system. As no major Cenozoic extensional tectonics superimposed on most of the late Mesozoic extensional system, numerous and various extension markers are still well preserved. Widespread late Mesozoic extensional sedimentary basins are amongst the most studied structures in East Asia owing to their coal and/or hydrocarbon potentialities (e.g. Liu, 1986; Watson et al., 1987; Ren et al., 2002; Zhang et al., 2010a; Li et al., 2012a). Besides, late

Mesozoic magmatic rocks cover large areas over East Asia (e.g. Wang, et al., 1998; Li, 2000; Wu et al., 2000, 2005a, 2005b, 2007; Zhang et al., 2010b). To the north-east of China, a pioneer and landmark geochronological study coupled with an age compilation have pointed out a “giant igneous event” settled between 130 and 120 Ma, leading to consider a coeval intense lithospheric thinning (Wu et al., 2005a). However, influence of magmatism on tectonic evolution remains rarely discussed for the late Mesozoic extension of East Asia. More recently, several MCCs have been recognised from Transbaikalia to the Jiaodong Peninsula, 2000 km apart (Fig. 1; e.g. Davis et al., 1996; Sklyarov et al., 1994; Webb et al., 1999; Darby et al., 2004; Liu et al., 2005; Lin and Wang, 2006; Donskaya et al., 2008; Daoudene et al., 2009; Charles et al., 2011a, 2012). While structure and kinematics of these MCCs are well-studied, the timing and duration of their development are often poorly constrained (Fig. 1). Accordingly, the precise timing and total duration of extensional process are also rarely estimated.

This paper focuses on the Jiaodong Peninsula (East China, Figs. 1 and 2) which experienced late Mesozoic NW-SE extensional tectonics (Charles et al., 2011a). Indeed, the common occurrence of MCCs, extensional shear zones, synkinematic and late isotropic granitic intrusions can be observed within a narrow zone and such a configuration constitutes a proper place to estimate the timing and duration of extensional tectonics. This paper primarily aims at bringing the first exhumation time-constraints for the Linglong MCC. Thus, conventional $^{40}\text{Ar}/^{39}\text{Ar}$ analyses were undertaken on both isotropic and deformed strained rocks where the synkinematic characters of successive mineral generations are texturally and chemically settled. Dating either other strained objects related to the same event and post-tectonic markers, this study also places constraints on the total duration of extensional tectonics recorded in the Jiaodong Peninsula. Coupled with a new geochronological compilation of extension markers throughout the East Asia, these new data allow discussing

the timing and the total duration of the continental extension history in this large-scale wide rift system. Moreover, relationships between wide rift system development and magmatism are discussed in the light of the “giant igneous event” that occurred in East Asia during late Mesozoic times. The evolution of the East Asia wide rift system is also compared to other highly stretched areas throughout the world (i.e. Basin & Range and Aegean regions).

2. Large-scale geological context and anatomy of the Jiaodong Peninsula

The East Asia wide rift system extends from South China to the Baikal Lake south-northwardly, and from the Japanese Islands to the Gobi desert east-westwardly. It forms a north-trending ~1500 km wide extensional band (Fig. 1; e.g. Davis et al., 1996; Ren et al., 2002; Meng, 2003; Liu et al., 2005; Lin and Wang, 2006; Zhai et al., 2007; Daoudene et al., 2009, 2011; Charles, 2010; Charles et al., 2011a, 2011b, 2012).

Late Mesozoic extensional basins are prominent geological and physiographical features of east-central Asia. Thanks to coal and oil exploration, these basins have been extensively studied in China (e.g. Liu, 1986; Watson et al., 1987). Sedimentation is characterised by coarse-grained continental deposits with calc-alkaline volcanic rocks that yielded a ca. 155 Ma age for the onset of sedimentation in the Songliao, Erlian, Hailar, Yingen or East Gobi basins (see references in Ren et al., 2002; Meng, 2003; Zhang et al., 2010a, 2011; Li et al., 2012a). Besides, the extensional character of the basins framework is attested by their overall half-graben geometry as displayed on seismic profiles. These are bounded by NE-SW trending normal faults and locally marked by growth-structures in the sedimentation (Chen et al., 1999; Ren et al., 2002; Lin et al., 2003; Meng, 2003). Tectonic subsidence lasted until 120-110 Ma, followed by a regional weak post-rift thermal subsidence (Ren et al., 2002; Meng, 2003). Nevertheless, in the Songliao basin (Fig. 1), thermal

subsidence was more important since it promoted deposits up to 6000 m from ~120 to ~70 Ma (Meng, 2003; Li et al., 2012a).

MCCs are the most prominent features of intense and localised extension into continental crust, and some of them have been described throughout East Asia such as: the Yagan-Onch Hayrhan MCC (Mongolia; Webb et al., 1999), the South Liaodong MCC, the Linglong MCC and the Gudaoling MCC (North China; Yin and Nie, 1996; Liu et al., 2005, Charles et al., 2011a, 2012), the Lüshan MCC (South China; Lin et al., 2000), the Buteel-Burgutoy and Ereendavaa MCCs (Mongolia; Mazukabzov et al., 2006; Donskaya et al., 2008; Daoudene et al., 2009) or the Zagan MCC (Russia; Donskaya et al., 2008). Kinematic analyses of the exhumation of these MCCs reveal a common overall NW-SE extensional tectonics throughout East Asia. Timing of the exhumation has already been studied for most of the MCCs (e.g. Davis et al., 1996; Webb et al., 1999; Yang et al., 2007; Lin et al., 2008) and ages, generally interpreted as cooling ages, all cluster at ca. 130-120 Ma (e.g. Lin and Wang, 2006; Daoudene et al., 2011; Lin et al., 2012).

Magmatic rocks are also particularly abundant throughout East Asia either as plutonic intrusions or as intercalated volcanic lavas within sedimentary basins. Emplacement ages for both plutonic and volcanic rocks are generally well documented and precisely constrained by HT thermochronological tools (e.g. Wang et al., 1998; Li, 2000; Wu et al., 2005a, b; Wang et al., 2006; Wu et al., 2007; Zhang et al., 2010b, Yang et al., 2012). Considering the apparent age clustering of plutonic rocks, Wu et al. (2005a) proposed the occurrence of a “giant igneous event” at around 130-120 Ma. However, a possible genetic link between this magmatic paroxysm and extension peak is still unclear.

The Jiaodong Peninsula is located in the eastern block of the North China Craton (see NCC on Fig. 1; Mattauer et al., 1985; Faure et al., 2003; Zhao et al., 2005; Zhang et al., 2009; Zhai and Santosh, 2011; Li et al., 2012b; Tam et al., 2012). Four main lithological groups are

recognised throughout the Jiaodong Peninsula (Fig. 2a): (1) Late Archaean gneisses, granulites, amphibolites and micaschists belonging to the Jiaodong Group (Tang et al., 2007; Jahn et al., 2008; Zhou et al., 2008); (2) Palaeoproterozoic mafic to felsic volcanic and sedimentary rocks metamorphosed to amphibolite-granulite facies (Jinshan and Fengzishan Groups; Wang, 1995; Tam et al., 2011; see Li et al., 2012b for details); (3) Late Jurassic and Early Cretaceous plutonic and metamorphic rocks (e.g. Luanjiahe, Kunyushan, Guojialing, Weideshan, Aishan and Haiyang massifs); and (4) Cretaceous volcano-sedimentary rocks of the Jiaolai basin (SBGMR, 1991). Late Mesozoic times were characterized by two distinct pulses in the magmatic activity (*s.l.*) at 160-150 Ma and especially at 130-120 Ma (Wang et al., 1998; Goss et al., 2010; Zhang et al., 2010b; Yang et al., 2012). The complex interplay among heat advection, deformation and fluid circulations is thus responsible for the genesis of giant gold deposits (e.g. Zhou and Lü, 2000; Yang et al., 2003; Li et al., 2008; Miao et al., 2012).

The Linglong complex is a NNE-SSW oriented massif located in the Pingdu-Laizhou-Zhaoyuan area (Fig. 2a). It is of ~60 km in length and ~30 km in width. Following Charles et al. (2011a), the Linglong complex can be divided into two main structural elements (Fig. 2b): (1) the Linglong MCC, which is intruded to the north by (2) the Guojialing synkinematic intrusion roofed by a main extensional shear zone.

3. Evolution of the Linglong complex

The detailed structural evolution of the Linglong complex area, which is beyond the scope of the present paper, was recently investigated by Charles et al. (2011a) in order to document the occurrence of a new MCC accompanied by subordinate extensional features all belonging to the East Asia wide rift system. Only main informations are summarised here.

3.1. Structural evolution of the Linglong MCC

The Linglong MCC (Fig. 2) is a NNE-SSW trending asymmetric dome. As typical cordilleran-type MCC (Crittenden et al., 1980), the Linglong MCC mainly exposes interfingered migmatites and anatectic granite in its core (Fig. 2b; Sang, 1984; SBGMR, 1991), separated to the east, with a master detachment zone, from Late Archaean metamorphic rocks to Early Proterozoic upper crustal units. Based on the Sr-Nd isotope ratios of 0.710498–0.712286 and $-20.46 - -21.12$ for $I_{Sr}(t)$ and $\epsilon_{Nd}(t)$, respectively, Zhou et al. (2003) have shown that the material source of the dome may be dominantly composed of “old crustal components”. These granitic rocks are essentially composed of a medium-grained (white-mica) monzogranite (Sang, 1984) whose crystallisation has been dated at 160-150 Ma (U/Pb ages on zircon; see Wang et al., 1998; Zhang et al., 2010b; Yang et al., 2012). Structurally above, finite strain increases over ~4 km from low strain domains in the core of the dome to a 0.5 km-thick ESE-dipping mylonitic zone, the Linglong detachment fault (LDF). The LDF is marked by a clear top-to-the-ESE sense of shear (Fig. 2b; Charles et al., 2011a). During the final exhumation stages, while numerous small-scale steeply-dipping normal faults overprint the ductile fabrics throughout the dome, the shear zone was reactivated under brittle conditions with a clear top-to-the-ESE kinematics.

3.2. The Guojialing shear zone and the late intrusions

The Guojialing shear zone (GSZ) lies to the north of the Linglong complex (Fig. 2). It forms a NNW-dipping, 25 km-long extensional ductile shear zone exhibiting a consistent top-to-the-NW sense of shear (Charles et al., 2011a). Thanks to the emplacement ages performed

on the synkinematic Guojialing intrusion (Fig. 2), its activity has been settled at ca. 130-126 Ma (Wang et al., 1998; Li et al., 2003; Yang et al., 2012). The core of the intrusion dominantly consists in porphyritic amphibole-biotite granodiorite. The Sr-Nd isotope ratios of 0.709361 – 0.711419 and -15.07 – -17.50 for $I_{Sr}(t)$ and $\epsilon_{Nd}(t)$, respectively, highlight a young enriched lithospheric mantle as partial melting source (Zhou et al., 2003). Here again, rock structure evolves north-westward from isotropic igneous rocks to mylonites over ~6 km (Fig. 2b). While this shear zone does not exhibit evidence of late brittle reactivation, spatially scattered normal brittle faults developed over the pluton and display a NW-SE striking subhorizontal stretching (Fig. 2b).

Subsequently, the overall Jiaodong Peninsula was intruded by pinkish-reddish granodioritic plutons (“PRG” in Fig. 2). Detailed field observations of the intrusive relationship between the plutons and country rocks combined with AMS study reveal the absence of coeval or late deformation of plutons (Charles et al., 2011b). Intrusion ages of these plutons (e.g. Weideshan, Aishan or Haiyang plutons) have been recently dated at 120-118 Ma by U/Pb analyses on zircon (Charles, 2010; Goss et al., 2010). These plutons then cool fast below the solidus in the upper crust at ca. 118 Ma as attested by the clustering of the whole spectrum of radiometric ages. Country rocks that were colder than ca. 250-300°C at that time behaved as a rigid body, resistant as the intrusion itself. Accordingly, PRG plutons are regarded as post-tectonic regional markers (Charles, 2010; Charles et al., 2011b). Besides, while gold mineralization event dates back to ca. 120 Ma (e.g. Li et al., 2003; Zhang et al., 2003), no link has currently been drawn between ore deposits and deformation.

Exhumation of the Linglong MCC below a top-to-the-ESE detachment fault, followed by the development of a top-to-the-NW extensional intracrustal shear zone demonstrates the persistence of horizontal stretching within the crust. However, up to now, timing and duration of extensional deformation is only fragmentary and still highly uncertain.

4. Sampling strategy

Sampling was performed following a two-fold strategy either for rock sampling in the field or mineral selection in the laboratory. Unstrained rocks were sampled to constrain the cooling age(s) through closure temperature (CT) of amphibole, white micas and biotite for the K/Ar isotopic system (Dodson, 1973; see also Harrison et al., 2009 for a recent review of the closure temperatures). In parallel, high-strain mylonites and brittle fault planes were sampled to determine the age of the deformation by dating synkinematic recrystallisations or synkinematic mineral blasteses (e.g. Turrillot et al., 2011). It is worth mentioning that $^{40}\text{Ar}/^{39}\text{Ar}$ method applied to synkinematic white-micas extracted from brittle faults allows dating crystallisation ages which occurred well below the CT (Dodson, 1973). Seven samples were then selected in the field from which ten mineral concentrates (and ultimately ten single-grains) were obtained (Fig. 2b, Tables 1 and 2). Samples 90-08, 165-08, 91-07 and 83-08 correspond to four white mica single-grains sampled from the Linglong MCC unstrained core, mylonites and brittle normal fault planes (Figs. 3a and 3b). Samples 167-08 and 139-08 consist in two pairs of amphibole and biotite picked from the isotropic facies of Guojialing granodiorite and mylonites of the GSZ, to the north, respectively (Figs. 3c and 3d). Sample 104-08 refers to both amphibole and biotite single-grains selected from the PRG pluton.

EPMA analyses (CAMECA SX50 electron microprobe) were carried out at the French Geological Survey (BRGM-ISTO common lab) to characterise the mineral chemistry. Analytic conditions were 15 kV accelerating voltage and 10 nA beam current using Fe_2O_3 (Fe), MnTiO_3 (Mn, Ti), diopside (Mg, Si), CaF_2 (F), orthoclase (Al, K), anorthite (Ca), albite (Na), and vanadinite (Cl) as standards. Despite a partial overlap, the white micas chemistry shows important compositional variability. Peculiar compositions can be related to the

different generations of white micas identified on textural grounds (Fig. 3e). Magmatic white micas (sample 90-08) which are preserved as clasts in mylonites (sample 165-08, Fig. 3a) are celadonite-poor (~3.12-3.18 c.p.f.u.) and paragonite-rich Ti-muscovite (Fig. 3e). Conversely, both recrystallised white micas in mylonites and newly formed white micas on fault planes (Fig. 3b) present higher celadonite content (~3.16-3.22 and 3.21-3.26 c.p.f.u., respectively) and higher X_{Mg} values. Figures 3f and 3g display the main results obtained for amphiboles and biotites. Amphiboles mostly stand in the field of the magnesio-hornblende (Leake et al., 1997) and contain from 0.8 to 1.6 K₂O wt% (Fig. 3f). Biotite analyses of all samples show a narrow range of chemical compositions, from 9.2 to 9.5 K₂O wt% and from 0.42 to 0.45 for X_{Fe} (Fig. 3g).

⁴⁰Ar/³⁹Ar measurements have all been performed at the Géosciences Montpellier geochronology laboratory. Conventional procedures for single-grain analyses are not reminded here in details and readers unfamiliar with the method and the analytical procedure are referred to recent publications (Heymes et al., 2010; Turrillot et al., 2011). Single crystals of white mica, amphibole and biotite were extracted from sample crushing (i.e. jaw crusher) or directly from the rock samples. After purification by a Frantz magnetic barrier separator, single grains were hand-picked from the 500-1000 µm fraction using a binocular microscope. Separates were washed in distilled water, acetone and ethanol before to be packed in individual aluminium foil packets for irradiation. Samples were irradiated in the McMaster nuclear reactor (Canada) together with aliquots of MMHb-1 flux monitors (520.4 ± 1.7 Ma; Samson and Alexander, 1987). The effects of interfering reactions with Ca and K were evaluated using the following correction factors obtained during a previous irradiation (McDougall and Harrison, 1999): (⁴⁰Ar/³⁹Ar)_K = 0.0156; (³⁹Ar/³⁷Ar)_{Ca} = 0.000651; (³⁶Ar/³⁷Ar)_{Ca} = 0.000254. Single crystals were degassed by means of a defocused continuous 50W CO₂ laser with a beam diameter of at least twice the size of the heated targeted grain.

After heating and gas cleaning, argon was introduced in a MAP215-250 mass spectrometer with a Nier ion source and a Johnston MM1 electron multiplier. Each analysis involved 5 min for gas extraction and cleaning and 8 min for data acquisition by peak switching from argon mass 40 to 36. Isotopic compositions were estimated by regression on 15-18 runs. System blanks were evaluated every two-three experiments.

For each experiment (Table 2), usual isotope corrections including blanks, mass discrimination, radioactive decay of ^{37}Ar and ^{39}Ar and irradiation-induced mass interference were applied. Errors reported for each step routinely take into account the errors introduced by these corrections as well as the analytical errors on signals. The uncertainty on the J -factor was propagated in the calculation of the error on the total age for each sample, equivalent to a K-Ar age. All ages are reported with one standard deviation (1σ) confidence level assuming an atmospheric composition for the initially trapped argon (i.e. $(^{40}\text{Ar}/^{36}\text{Ar})_i = \text{ca. } 295.5$; McDougall and Harrison, 1999).

5. $^{40}\text{Ar}/^{39}\text{Ar}$ results and ages interpretation

All analysed samples showed a straightforward behaviour during step-heating with plateau-segments corresponding to more than 74% of gas released for amphiboles and 89% for white micas and biotite. Results are presented in Table 1 and $^{40}\text{Ar}/^{39}\text{Ar}$ age spectra are displayed in Figure 4. Besides, thermochronological age constraints are included into a presumed cooling path.

White micas from sample 90-08 (Fig. 4a) were picked in the core of the Linglong MCC, structurally far below the detachment fault, where the lack of significant sub-solidus deformation well preserves partial melting textures (i.e. interfingering of anatectic granite within the migmatites). This white mica sample, characterised by a clear chemical magmatic

signature (Fig. 3e) yielded a well-defined plateau age of 142.81 ± 1.43 Ma (Fig. 4a). These features argue that this age would approximate a cooling age through temperatures required for intra-crystalline retention of radiogenic argon in white micas at T of $\sim 450 \pm 50^\circ\text{C}$ (Villa, 1998, Harrison et al., 2009).

White micas from the LDF mylonites (165-08; Fig. 4a), that derive from the same protolith yielded a plateau age spectrum of 133.98 ± 1.47 Ma. As demonstrated by a clear secondary character either on a textural ground or by contrasted chemical composition (Fig. 3e), this age cannot simply reflect a cooling age. Conversely, it could correspond to the last mineral recrystallisations during ductile deformation, just above the ductile-brittle transition at about 350°C (e.g. Hyndman et al., 1997), and therefore rather defining the lower bound of the presumed closure temperature of phengite (Hames and Browring, 1994; Hames and Cheney, 1997; Villa, 1998). This ca. 9 Ma younger age than the overall cooling of the dome indicates that ductile shearing along the LDF was still active at that time. Some grain-size effects are discarded since dated white micas are texturally and chemically distinct from magmatic clasts.

Two white micas sampled from late brittle fault planes (Fig. 4b) yielded plateau age spectra of 128.19 ± 1.36 Ma (sample 83-08) and 127.7 ± 1.34 Ma (sample 91-07). These white mica populations appear as synkinematic crystallisations on brittle planes as they appear as sheared rosette-shaped aggregates of large muscovite flakes (Fig. 3b) that cannot be confounded with inherited clasts (i.e. older magmatic grains). Besides, synkinematic fluid circulations along the fault planes yielded an intense sericitisation of the wall-rock (Fig. 3b). Since white micas blastesis occurred well below the closure temperature for white micas, these ages reflect crystallisation ages and unequivocally place constraints on the timing of the brittle deformation.

The paired amphibole and biotite from the same sample of unstrained rocks from the Guojialing intrusion (sample 167-08, Fig. 4c) yielded plateau ages of 130.23 ± 1.96 Ma and 124.39 ± 1.36 Ma, respectively. This last result is consistent with previously published ca. 124.0 ± 0.4 Ma $^{40}\text{Ar}/^{39}\text{Ar}$ ages on biotite (Li et al., 2003). Since sample is devoid of strain, these ages must represent cooling ages through the closure temperatures of amphibole ($\sim 550 \pm 50^\circ\text{C}$) and biotite ($\sim 350 \pm 30^\circ\text{C}$; e.g. Villa, 1998).

Amphibole and biotite from the GSZ mylonites (sample 139-08; Fig. 4d) yielded plateau ages of 124.12 ± 1.79 Ma and 123.16 ± 1.54 Ma, respectively. These younger ages, however, may rather correspond to the latest mineral recrystallisations during mylonitisation. Indeed, strain amount is so intense in these rocks that amphiboles thus behaved as an open-system for temperatures as low as the biotite closure temperature. It is noteworthy that last mineral recrystallisations, and thus argon diffusion, occurred while the intrusion crossed the lower bound of the ductile-brittle transition ($\sim 350^\circ\text{C}$; e.g. Hyndman et al., 1997).

$^{40}\text{Ar}/^{39}\text{Ar}$ ages on amphibole and biotite performed on an isotropic pinkish-reddish granodioritic sample (104-08; Fig. 4e), intruded into the Linglong MCC and cutting across its ductile pervasive structures, yielded 121.74 ± 3.61 Ma and 118.79 ± 1.35 Ma plateau ages, respectively. These rocks, devoid of strain and characterised by initial magmatic texture, fit with the thermochronology hypothesis (Dodson, 1973) that explains these ages as the time elapsed since the rock cooled below ca. 550°C and 350°C , respectively (Harrison et al., 2009).

6. Tectonic evolution of the Linglong complex

In the Linglong MCC, direct and unambiguous dating of partial melting event is currently lacking but the ca. 160-150 Ma U/Pb ages on zircon (Wang et al., 1998) obtained from anatectic granites in spatial and structural close relationship with migmatites may

document this stage. Besides, at the scale of the wide rift system, Upper Jurassic also corresponds to the development of extensional basins throughout East Asia (e.g. Songliao, Erlian or East Gobi basins) with particularly high tectonic subsidence rates related to normal faulting (Ren et al., 2002; Meng, 2003; Li et al., 2012a). This earliest stage of MCCs development may thus correspond to the “upper crustal necking” phase of Tirel et al. (2008) with the coeval development of basins at crust surface and the effect of partial melting in the lowermost crust. Subsequently and after a rather long period of slow cooling rates, the Linglong MCC lower unit exhumed and cooled below $\sim 450 \pm 50^\circ\text{C}$ at ~ 143 Ma while the LDF still localised ductile strain at least until ~ 134 Ma (Fig. 4f). Finally, the brittle deformation as evidenced along the main detachment zone marks the end of the movement along the LDF, at ca. 128 Ma, with the same kinematics. The exhumation history of the Linglong MCC, as recorded by the K/Ar isotopic system, thus lasted over more than 15 My (Fig. 4f). If considering the ca. 160-150 Ma ages as the onset of the MCC development, during upper crustal necking stages, the total duration of the Linglong MCC emplacement then probably lasted over more than 25 My.

Development of the Linglong MCC accompanied by strain localisation along the LDF is followed by ductile shearing along an intracrustal extensional shear zone striking ENE and roofing the Guojialing synkinematic pluton (Charles et al., 2011a). Kinematical observations made along this shear zone show the persistence of a common NW-SE extensional regime during the entire uprising evolution of the Linglong MCC and the Guojialing pluton intrusion (Charles et al., 2011a). Structural interpretations for the western Jiaodong area are consistent with the NW-SE overall extensional tectonics experienced by the whole eastern Asia during late Mesozoic times. Combined with published U/Pb ages on zircon (Wang et al., 1998), our new $^{40}\text{Ar}/^{39}\text{Ar}$ results show a fast cooling rate of the order of $100^\circ\text{C}/\text{My}$ for the Guojialing intrusion, from its emplacement settled at 130-126 Ma (Wang et al., 1998) to its cooling

below $\sim 350^{\circ}\text{C}$ at ca. 124 Ma, consistent with an emplacement within the upper crust (Fig. 4g). Besides, tectonic denudation and strain localisation along the GSZ lasted until ~ 123 Ma.

Finally, PRG isotropic plutons emplaced at 122-118 Ma (Charles, 2010; Charles et al., 2011b) and cooled extremely fast, most probably within upper crustal levels, down to $\sim 350 \pm 50^{\circ}\text{C}$ at 118 Ma (Fig. 4g). Intrusion of these regionally unstrained plutons definitely marks out the end of significant strain during late Mesozoic times in the Jiaodong Peninsula. Following the protracted exhumation history of the Linglong MCC between presumably 160-150 Ma and 128 Ma, extension in the Jiaodong Peninsula thus persisted until 123 Ma.

Duration of extensional tectonics can then be crudely bracketed to more than 30 My from 160-150 Ma to 122-118 Ma, while exhumation of MCCs in neighbouring geological domains (e.g. Liaodong Peninsula) still continued until 115-100 Ma (Yang et al., 2007; Lin et al., 2011). This point is discussed below.

7. Discussion

Wide rift systems are defined as a uniform crustal and lithospheric mantle thinning over a width greater than the lithosphere thickness (Buck, 1991). They display pervasive stretching as crust behaves as ductile for its most parts, with a particularly thin upper brittle crust (Buck, 1991). Lower ductile crust flow leads to a rather flat horizontal Moho (e.g. resulting crust thickness between 30-35 km for the entire Basin and Range region). This peculiar rheology of the lithosphere favours MCCs development, which concentrates a large proportion of the strain amount recorded into the upper continental crust (Brun and Van Den Driessche, 1994; Tirel et al., 2008; Charles et al., 2011a). Furthermore, magmatism is often associated with wide rift systems and as emphasizing lithosphere weakening. Magmatism could have an important role during continental extension (Coney and Harms, 1984; Lynch

and Morgan, 1987; Péron-Pinvidic et al., 2009; Rey et al., 2009a, b). In wide rift systems, amount of stretching and strain rates show variations in both time and space, as demonstrated by geochronological syntheses in Basin & Range and Aegean regions (see references below), and could have a direct link with magmatism.

East Asia is a typical “wide rift system” characterised by a ~1500 km wide zone affected by pervasive NW-SE extension developed during late Mesozoic times (e.g. Ren et al., 2002; Meng, 2003; Lin and Wang, 2006; Zhai et al., 2007; Charles et al., 2011a, 2012). Magmatic activity is particularly well expressed in East Asia as shown by the abundance of plutonic intrusions and volcanic massifs (Fig. 1). The peak of magmatism, dated at ca. 130-120 Ma (Fig. 5a), has been proposed to correspond to the extension paroxysm (Wu et al., 2005a; Daoudene et al., 2011). However, such an assumption is not straightforward when comparing, at local-scale, structures development and magmatism, as discussed below. In the East Asia wide rift system, MCCs, extensional sedimentary basins, sheared and isotropic plutons which do not mark the same finite strain amount locally undergone by the continental crust, are distributed in time and spatially scattered. Thus, a comparison between timing of the extensional deformation and of magmatism throughout East Asia allows discussing the genetic link between both processes in wide-rift continental extension processes (Fig. 5). A compilation of initiation ages as well as total exhumation duration has been made for several MCCs throughout well-known wide rift systems, including East Asia (Fig. 6). This compilation unambiguously highlights the coexistence of contrasted MCC-types (slow and fast MCC) and, consequently, a clear diachronous character of the extension within the East Asia wide rift system. Such a variability of continental extension amount, in time and space, is finally compared to two others extended domains (i.e. Basin & Range, Aegean) according to available published syntheses (Miller et al., 1988; Vanderhaeghe et al. 1997; Wawrzenitz and Krohe 1998; Vanderhaeghe et al. 1999; McGrew et al. 2000; Keay et al. 2001; Lorencak

et al. 2001; Norlander et al., 2002; Ring et al. 2003; Isik et al. 2004; Ring and Collins, 2005; Brichau et al. 2006; Duchêne et al. 2006; Sullivan and Snoke 2007).

7.1. The East Asia wide rift system

7.1.1. Timing and duration of extensional tectonics

Figure 5 displays a compilation of geochronological data on MCCs development, magmatic pulses and extensional basins tectonic subsidence throughout East Asia. In the light of this compilation, most of the major sedimentary basins in East Asia (Fig. 5b; i.e. Songliao, East Gobi, Erlian, Hailar or Yingen basins; Ren et al., 2002; Meng, 2003) began to develop during Late Jurassic times (i.e. J₃: 160-150 Ma) in response to NW-SE extension and pervasive normal faulting (e.g. Songliao basin, Chen et al., 1999; Lin et al., 2003; Li et al., 2012a). The onset of continental extension in the East Asia wide rift system may have thus started during Late Jurassic at ca. 160-150 Ma (Fig. 5b). During this rather long-lived extensional period, development of MCCs, and ultimately extensional strain amount, occurred continuously and thus appears highly diachronous in East Asia (Fig. 5b). For example, the final exhumation of the Linglong MCC, at ca. 143 Ma, appears coeval with the development of the Gudaoling MCC (Charles, 2010; Charles et al., 2012) and Ereendavaa MCC (Daoudene et al., 2009, 2011) but is clearly older than the development of most MCCs of eastern China, such as the South Liaonan MCC (Liu et al., 2005; Lin and Wang, 2006; Yang et al., 2007; Lin et al., 2011). Moreover, plutons that emplaced during this period (i.e. synkinematic plutons) yield also interesting conclusions since some are sheared, while some others are devoid of significant strain (Fig. 5). Therefore, extensional strain during late Mesozoic appears heterogeneously distributed in both time (from 160 to 100 Ma) and space. Indeed, strain is most concentrated along rather localised structures (e.g. detachment faults) which separate

large crustal segments devoid of significant deformation. Besides, the estimation of the ca. 60 My duration for continental extension in East Asia could be longer since crustal stretching has been evidenced during Cenozoic times all along East Asian continental margin as in the Bohai basin, South China Sea and Japan Sea (Jolivet et al., 1994; Ren et al., 2002) or in the Baikal rift (Sengör and Burke, 1978; Logatchev and Zorin, 1987; Jolivet et al., 2009b). However, even if the NW-SE stretching direction remained stable through time, is there a real continuity of continental extension between late Mesozoic and Tertiary?

7.1.2. Magmatism vs. extension: a conspicuous yet possibly opposed link

Extensional processes can be favoured by partial melting and widespread magmatism which reduce lithosphere strength, emphasizing deformation and strain localisation (Van der Molen and Paterson, 1979; Reynolds and Rehrig, 1980; Coney and Harms, 1984; Lynch and Morgan, 1987; see synthesis in Handy and Brun (2004)). In eastern China, strong magmatic activity, defined as the “giant igneous event”, occurred dominantly at 130-120 Ma suggested as being coeval to lithospheric thinning (Fig. 5a; Wu et al., 2005a, b; Menzies et al., 2007). Coincidence of the age of this magmatic pulse and recent thermochronological time-constraints on the exhumation of some MCCs (e.g. the South Liaonan MCC) has led to consider this period as corresponding to the Mesozoic extension climax in East Asia (e.g. Wu and Sun, 1999; Daoudene et al., 2011).

The Yagan-Onch Hayrhan, Yiwulüshan, South Liaonan or Gudaoling MCCs development, for example, are partially or totally coeval with the “giant igneous event” magmatic peak (Fig. 5). However, the above discussion shows that extension may have started well before, from ca. 160-150 Ma, as evidenced by the widespread development of extensional sedimentary basins (Fig. 5b; Ren et al., 2002; Meng, 2003), thus characterised by

high tectonic subsidence rates and by the emplacement of large volumes of calc-alkali interlayered lavas (Ren et al., 2002; Meng, 2003). This is strengthened by the development of MCCs such as the Linglong, the Gudaoling MCC (Charles, 2010; Charles et al., 2012) or the Ereendavaa MCC (Daoudene et al., 2009, 2011) which occurs prior to the Early Cretaceous “giant igneous event” settled at ca. 130-120 Ma (Fig. 5). Conversely, while several MCCs emplaced in East Asia during the magmatic pulse, some areas did not experience such large stretching. For example in the Jiaodong Peninsula, this period is only characterised by the emplacement of sheared pluton such as the Guojialing synkinematic intrusion between 128 and 124 Ma (Fig. 5). At larger scale, isotropic intrusions (Fig. 5; i.e. PRG plutons, Aishan, Badaling, Dahaituo, Xuejiashiliang) denoting a local relative atectonic setting clearly emplaced during the magmatic pulse (~130-119 Ma; Yang et al., 2007; Charles et al., 2011b).

Geodynamic cause(s) for the late Mesozoic extension in East Asia is still hotly debated (see references in Zhai et al., 2007; Charles, 2010). These new results show that extensional processes span at least from ca. 160 to 100 Ma. Such duration of ca. 60 My promotes a rather long process for extension as the progressive slab retreat of the Palaeo-Pacific plate from 160 Ma onward (Maruyama et al., 1997; Bartolini and Larson, 2001; Zhai et al., 2007), instead of instantaneous events or as the convective removal (Huang and Zhao, 2006; Lin and Wang, 2006; Wang et al., 2006; Chen, 2010) or mantle plume (Okada, 1999; Zhao et al., 2007) at 130-120 Ma. It is therefore tempting to propose that the magmatic pulse, characterised by a quite sudden surge of temperature at 130-120 Ma, may have been favoured by extension. Age clustering of both numerous magmatic intrusions and some MCCs would be the result of a feed-back relationship where, in turn, partial-melting thus may have triggered extension.

Besides, the present study points out that both fast and slow MCCs developed throughout East Asia during the overall Mesozoic extension period. Rey et al. (2009a)

mention that such feature may be partly linked to the volume of melt involved during deformation. Variations in magmatic activity during the 60 My long continental extension history of East Asia could thus also control the change in structural style observed within the crust and, in particular, within MCCs.

7.2. MCCs and wide rift systems in the world

Recent thermomechanical numerical experiments on the development of MCCs reveal that fundamental petrological and structural differences can be established between two end-member of MCC-types: those developed under fast and localised extension (i.e. of the order of cm/yr) or, conversely, those developed under slower extension (Rey et al., 2009a, b). Here, a new compilation for the duration of MCC development, throughout different continental extended domains in the world, is presented in Figure 6. Typical durations range from less than 10-12 My long for the “fast” MCCs, such as Shuswap, Naxos and the North Menderes (Vanderhaeghe et al., 1997, 1999; Keay et al., 2001; Lorencak et al., 2001; Norlander et al., 2002; Ring et al., 2003; Isik et al., 2004; Ring and Collins, 2005; Brichau et al., 2006; Duchêne et al., 2006) to more than 60 My for the “slow” MCCs, such as South Rhodope, Ruby Mountains and the Snake Range (Miller et al., 1988; Wawrzenitz and Krohe 1998; McGrew et al., 2000; Sullivan and Snoke, 2007; Burg, 2012).

In the light of our new $^{40}\text{Ar}/^{39}\text{Ar}$ and existing age constraints, the ca. 25 My-long development of the Linglong MCC falls in the range of the rather fast MCC-type (Fig. 6) with which it shares typical features (Rey et al., 2009a, b) including a high melt fraction and a weakly deformed core (Charles et al., 2011a). Amazingly, the Gudaoling MCC (Liaodong Peninsula), where partial-melting event is settled at ca. 157 Ma, developed as a rather slow MCC-type with a duration of ca. 50 My (Yang et al., 2008; Charles, 2010; Charles et al.,

2012). Besides, the South Liaonan MCC, its northern structural prolongation, is characterised by coeval decompression and cooling along a medium thermal gradient (ca. 25°C/My; Lin et al., 2011). Even if precise time-constraints are still needed for other MCCs throughout East Asia, this study points out that the Mesozoic East Asia wide rift system displays both fast and slow types of MCCs, indicating tempo variations during the extension history (Rey et al., 2009a).

In the light of our compilation, this point appears common to the others wide rift systems in the world. According to a recent synthesis (Jolivet and Brun, 2010), post-orogenic extensional tectonics in the Aegean realm may have started around 55-45 Ma in the Rhodope massif (e.g. Wawrzenitz and Krohe, 1998; see synthesis in Burg, 2012) and last increments of ductile-brittle deformation were recorded over major detachments planes some 9-8 Ma ago (e.g. Brichau, et al., 2006; Grasemann et al., 2009). In this area, MCCs, such as Naxos and South Rhodope massifs (Fig. 6), exhibit contrasted features that develop under different conditions of melt fraction and extension rates (e.g. Vanderhaeghe, 2004). In the Naxos migmatite-cored dome, crystallisation of migmatites leucosomes and synkinematic granitoids occurred between 20 and 12 Ma (Keay et al., 2001) and were followed by a rapid cooling through amphibole and micas $^{40}\text{Ar}/^{39}\text{Ar}$ closure temperatures at ~11 Ma, and through zircon and apatite fission-tracks annealing temperatures between 11 and 8 Ma (Brichau et al., 2006; Duchêne et al., 2006). This fast cooling rate is ascribed to the fast exhumation and to efficient tectonic denudation below the North Cycladic Detachment Structure and strongly argues for fast local extensional strain rates. In contrast, the South Rhodope MCC recorded a protracted exhumation history that may started 51-39 Ma ago (Wawrzenitz and Krohe, 1998) and continued from 26 Ma to 8 Ma (Weingartner and Hejl, 1994; Wawrzenitz and Krohe, 1998), when the bulk of MCC development occurred (Burg, 2012). Thus, South Rhodope MCC suggests slower extensional and probably varying strain rates compared to the Naxos MCC.

In the Aegean realm, both fast and slow MCCs (e.g. Naxos and South Rhodope, respectively) occurred within a narrow area and suggest that extensional strain rates are thus heterogeneously distributed in time and space.

Similar conclusions were already proposed in the Basin and Range province where Axen et al. (1993) have proposed a compilation of exhumation constraints for MCCs throughout this wide rift system (Canada, United States and Mexico). Again, this synthesis highlights that extensional strain rates are heterogeneously expressed in time and space. Indeed, wide rift system is initiated earlier to the north in Canada, Washington and Idaho states (Eocene), compared to the south, in Nevada and Arizona states and Mexico (Oligocene to even Miocene). Furthermore, the Basin and Range province exhibits contrasted fast and slow MCC-types as exemplified by the Shuswap and Ruby Mountains MCCs as possible examples of type-example of fast then slow MCCs (Rey et al., 2009a).

Coexistence of slow and fast MCC-types in wide rift systems (Rey et al., 2009a) is then confirmed by this study. The variety in styles observed within MCCs can possibly be linked to the tempo and duration of extensional deformation, as well as the volume of melt involved.

8. Conclusions

New $^{40}\text{Ar}/^{39}\text{Ar}$ analyses have been performed either on unstrained rocks, mylonites or brittle fault planes in a key area pertaining to the East Asia wide rift system. This approach allows constraining both cooling ages of the K/Ar isotopic system as well as deformation ages. Thereby, the overall cooling of the Linglong MCC below $\sim 450^\circ\text{C}$ occurred at 143 Ma whereas mylonitization and brittle deformations over the associated detachment fault lasted until to 128 Ma. The Guojialing synkinematic pluton subsequently emplaced and cooled fast

down from ~128 Ma to 124 Ma below an intracrustal shear zone which crossed the ductile-brittle transition at ca. 123 Ma. The ages of 120-118 Ma, ascribed to the fast cooling of unstrained plutons mark the end of extension at the scale of the region. Beyond the regional impact of these pioneer data on the Linglong complex evolution, these results allow drawing the following conclusions:

1. Duration for the Linglong MCC development is crudely estimated to ca. 25 My. The Linglong MCC thus appears as a rather fast MCC-type as it closely matches numerical modelling results of fast extension in the presence of melt (Rey et al., 2009a, b). Moreover, such fast MCC seems to coexist, in close vicinity, with slow then fast MCCs such as the Gudaoling MCC which developed after a most probable common partial melting event at ca. 160 Ma (Charles, 2010; Charles et al., 2012).

2. Continental extensional tectonics appears heterogeneously distributed in space and time in East Asia. Spatial heterogeneity is characterised by highly deformed areas (MCCs) that bound larger weakly deformed to unstrained zones characterised by synkinematic and /or unstrained plutons. In turn, the temporal heterogeneity is marked by the continuous development of extensional strain markers from ca. 160-150 Ma to ca. 100 Ma as viewed by the diachronous development of MCCs throughout East Asia that does not always match the Early Cretaceous “giant igneous event”.

3. Since continental extension started earlier than magmatic pulse, partial melting may have been favoured by crustal stretching. Subsequently, introduction of a large volume of melt in the continental crust may have favoured a feed-back relationship which maintained specific rheological properties, promoting continental extension through time.

4. The resulting ca. 60 My total duration for extensional tectonics is best explained by a rather long and continuous process. It is therefore tempting to propose the progressive slab

retreat of the Palaeo-Pacific plate from 160 Ma as the more likely phenomenon to explain the tectonic evolution.

5. A compilation at the scale of the whole wide rift system allows discriminating the coexistence of both slow and fast MCC-types emphasizing a heterogeneous distribution of extensional strain rates in both time and space as also observed in other wide rift systems.

Acknowledgments

This research was funded by the French national “Failles-Fluides-Flux” project supported by the INSU-CNRS, the Chinese National 973 Project No 2009CB825008 and the contribution of the ISTO (CNRS UMR 7327). We present our special thanks to the staff of Géosciences Montpellier together with P. Turrillot for their help during $^{40}\text{Ar}/^{39}\text{Ar}$ analysis. Dr Wei Lin is greatly acknowledged for its assistance and discussion in the field. We gratefully acknowledge Dr D. Gapais, Dr Y.J. Wang, Dr W. Xiao (Associated editor) and Pr. M. Santosh (Editor-in-Chief) for their constructive remarks that improved our manuscript.

References

Axen, G.J., Taylor, W.J., Bartley, J.M., 1993. Space-time patterns and tectonic controls of Tertiary extension and magmatism in the Great Basin of the western United States. *Geological Society of America Bulletin* 105, 56-76.

Bartolini, A., Larson, R.L., 2001. Pacific microplate and the Pangea supercontinent in the Early to Middle Jurassic. *Geology* 29, 735-738.

BBGMR, 1991. Regional geology of the Beijing Municipality. Geological Memoirs of Ministry of Geology and Mineral Resources, 27, Geological Publishing House, Beijing, 598 p.

Brichau, S., Ring, U., Ketcham, R.A., Carter, A., Stockli, D., Brunel, M., 2006. Constraining the long-term evolution of the slip rate for a major extensional fault system in the central Aegean, Greece, using thermochronology. *Earth and Planetary Science Letters* 241, 293-306.

Brun, J.P., Sokoutis, D., Van Den Driessche, J., 1994. Analogue modeling of detachment fault systems and core complexes. *Geology* 22, 319-322.

Brun, J.-P., Van Den Driessche, J., 1994. Extensional gneiss dome and detachment fault systems: structure and kinematics. *Bulletin de la Société Géologique de France* 165, 519-530.

Brun, J.P., 1999. Narrow rifts versus wide rifts: inferences for the mechanics of rifting from laboratory experiments. *Philosophical Transactions of the Royal Society of London, Series A* 357, 695-712.

Buck, W.R., 1991. Modes of continental lithospheric extension. *Journal of Geophysical Research* 96(B12), 161-178. doi:10.1029/91JB01485.

Burg, J.-P., 2012. Rhodope: From Mesozoic convergence to Cenozoic extension. Review of petro-structural data in the geochronological frame. In: (ed.) Skourtsos, E., Lister, G.S., *The Geology of Greece*. *Journal of the Virtual Explorer* 42.

Charles, N., 2010. Mechanisms of Mesozoic continental extension in East Asia. PhD thesis, Université d'Orléans, 476 p.

Charles, N., Gumiaux, C., Augier, R., Chen, Y., Zhu, R. and Lin, W., 2011a. Metamorphic Core Complex vs. Synkinematic pluton in continental extension setting: Insights from key structures (Shandong Province, eastern China). *Journal of Asian Earth Sciences* 40, 261-278.

Charles, N., Chen, Y., Augier, R., Gumiaux, C., Lin, W., Faure, M., Monié, P., Choulet, F., Wu, F.Y., Zhu, R., Wang, Q., 2011b. Palaeomagnetic constraints from granodioritic plutons (Jiaodong Peninsula): New insights on Late Mesozoic continental extension in eastern Asia. *Physics of the Earth and Planetary Interiors* 187, 276-291.

Charles, N., Gumiaux, C., Augier, R., Chen, Y., Faure, M., Lin, W., Zhu, R., 2012. Metamorphic Core Complex dynamics and structural development: Field evidences from the Liaodong Peninsula (China, East Asia). *Tectonophysics* 560, 22-50.

Chen, J., Cai X., Lin, C., Wang, H., Lei, M., 1999. Tectonic characteristics and episodic evolution of the northern fault depression in Songliao Basin. *Acta Petrologica Sinica* 20, 14-18 (in Chinese with English abstract).

Chen, L., 2010. Concordant structural variations from the surface to the base of the upper mantle in the North China Craton and its tectonic implications. *Lithos*, doi:10.1016/j.lithos.2009.12.007.

Coney, P.J., Harms, T.A., 1984. Cordilleran metamorphic core complexes: Cenozoic extensional relics of Mesozoic compression. *Geology* 12, 550-554.

Corti, G., Bonini, M., Conticelli, S., Innocenti, F., Manetti, P., Sokoutis, D., 2003. Analogue modelling of continental extension: a review focused on the relations between patterns of deformation and the presence of magma. *Earth Science Reviews* 63, 169-247.

Crittenden, M.D., Coney, P.J., Davis, G.H., 1980. Tectonic significance of metamorphic core complexes of the North American Cordillera. *Memories of Geological Society of America* 153.

Daoudene, Y., Gapais, D., Ledru, P., Cocherie, A., Hocquet, S. and Donskaya, T.V., 2009. The Ereendavaa Range (north-eastern Mongolia): an additional argument for Mesozoic extension throughout eastern Asia. *International Journal of Earth Sciences* 98, 1381-1393.

Daoudene, Y., Ruffet, G., Cocherie, A., Ledru, P., Gapais, D., 2011. Timing of exhumation of the Ereendavaa metamorphic core complex (north-eastern Mongolia) - U-Pb and $^{40}\text{Ar}/^{39}\text{Ar}$ constraints. *Journal of Asian Earth Sciences* (in press), doi:10.1016/j.jseaes.2011.04.009.

Darby, B.J., Davis, G.A., Zhang, X., Wu, F., Wilde, S., Yang, J., 2004. The newly discovered Waziyu metamorphic core complex, Yiwulüshan, western Liaoning province, Northwest China. *Earth Science Frontiers* 11, 145-155.

Davis, G.H. and Coney, P.J., 1979. Geologic development of the Cordilleran metamorphic core complexes. *Geology* 7, 120-124.

Davis, G.A., Qian, X., Zheng, Y., Yu, H., Wang, C., Mao, T.H., Gehrels, G.E., Muhammad S., Fryxell, J.E., 1996. Mesozoic deformation and plutonism in the Yunmeng Shan: A Chinese metamorphic core complex north of Beijing, China. In: The tectonic evolution of Asia (A. Yin & T.A. Harrison, eds). Cambridge University Press, New York, 253-280.

Davis, G.A., Zheng, Y., Wang, C., Darby, B.J., Zhang, C., Gehrels, G., 2001. Mesozoic tectonic evolution of the Yanshan fold and thrust belt, with emphasis on Hebei and Liaoning provinces, northern China. Geological Society of America Memoirs 194, 171-197.

Dodson, M., 1973. Closure temperature in cooling geochronological and petrological systems. Contributions to Mineralogy and Petrology 40, 259-274.

Donskaya, T.V., Windley, B.F., Mazukabzov, A.M., Kröner, A., Sklyarov, E.V., Gladkochub, D.P., Ponomarchuk, V.A., Badarch, G., Reichow, M.K., Hegner, E., 2008. Age and evolution of late Mesozoic metamorphic core complexes in southern Siberia and northern Mongolia. Journal of Geological Society of London 165, 405-421.

Duchêne, S., Aïssa, R., Vanderhaeghe, O., 2006. Pressure-Temperature-time Evolution of Metamorphic Rocks from Naxos (Cyclades, Greece): Constraints from Thermobarometry and Rb/Sr dating. Geodinamica Acta 19, 299-319.

England, P., 1983. Constraints on extension of continental lithosphere. Journal of Geophysical Research 88, 1145-1152.

Faure, M., Lin, W., Monié, P., Le Breton, N., Poussineau, S., Panis, D. and Deloule, E., 2003. Exhumation tectonics of the ultrahigh-pressure metamorphic rocks in the Qinling orogen in east China : New petrological-structural-radiometric insights from the Shandong Peninsula. *Tectonics* 22, 1018.

Gautier, P., Brun, J.P., Moriceau, R., Sokoutis, D., Martinod, J., Jolivet, L., 1999. Timing, kinematics and cause of Aegean extension: a scenario based on comparison with simple analogue experiments. *Tectonophysics* 315, 31-72.

Gautier, P., Brun, J.P., Jolivet, L., 1993. Structure and kinematics of upper Cenozoic extensional detachment on Naxos and Paros (Cyclades Islands, Greece). *Tectonics* 12, 1180-1194.

Goss, S.C., Wilde, S.A., Wu, F.Y., Yang, J.H., 2010. The age, isotopic signature and significance of the youngest Mesozoic granitoids in the Jiaodong Terrane, Shandong Province, North China Craton. *Lithos* 120, 309-326.

Grasemann, B., Schneider, D.A., Iglseder, C., Tschegg, C., 2009. Characteristics of low-angle normal faulting in Serifos (Western Cyclades, Greece). *Trabajos de Geologia* 29, 329-331.

Hames, W. E., Browring, S. A., 1994. An empirical evaluation of the argon diffusion geometry in muscovite. *Earth and Planetary Science Letters* 124, 161-167.

Hames, W. E., Cheney, J. T., 1997. On the retention of $^{40}\text{Ar}^*$ on the muscovite during reheating events. *Geochimica and Cosmochimica Acta* 68, 3863-3872.

Handy, M.R., Brun, J.P., 2004. Seismicity, structure and strength of the continental lithosphere. *Earth and Planetary Science Letters* 223, 427-441.

Harrison, T. M., Celerier, J., Aikman, A.B., Hermann, J., Heizler, M.T., 2009. Diffusion of Ar in muscovite. *Geochimica et Cosmochimica Acta* 73 1039-1051.

Heymes, T., Monié, P., Arnaud, N., Pêcher, A., Bouillin, J.P., Compagnoni, R., 2010. Alpine tectonics in the Calabrian-Peloritan belt (southern Italy): New $^{40}\text{Ar}/^{39}\text{Ar}$ data in the Aspromonte Massif area. *Lithos* 114, 451-472.

Huang, J., Zhao, D., 2006. High-resolution mantle tomography of China and surrounding regions. *Journal of Geophysical Research* 111, doi:10.1029/2005JB004066.

Hyndman, R. D., Yamano, M., Oleskevich, D. A., 1997. The seismogenic zone of subduction thrust faults. *Island Arc* 6, 244-260.

Isik, V., Tekeli, O., Seyitoglu, G., 2004. The $^{40}\text{Ar}/^{39}\text{Ar}$ age of extensional ductile deformation and granitoid intrusion in the northern Menderes core complex: implications for the initiation of extensional tectonics in western Turkey. *Journal of Asian Earth Sciences* 23, 555-566.

Jolivet, L., Takami, K., Fournier, M., 1994. Japan Sea, opening history and mechanism: A synthesis. *Journal of Geophysical Research* 99, 22237-22259.

Jolivet, L., Faccenna, C., Piromallo, C., 2009a. From mantle to crust: Stretching the Mediterranean. *Earth and Planetary Science Letters* 285, 198-209.

Jolivet, M., De Boisgrollier, T., Petit, C., Fournier, M., Sankov, V.A., Ringenbach, J.C., Byzov, L., Miroshnichenko, A.I., Kovalenko, S.N., Anisimova, S.V., 2009b. How old is the Baikal rift zone? Insights from apatite fission track thermochronology. *Tectonics* 28, TC3008, doi:10.1029/2008TC002404.

Jolivet, L., Brun, J.P., 2010. Cenozoic geodynamic evolution of the Aegean. *International Journal of Earth Sciences* 99, 109-138.

Keay, S., Lister, G., Buick, I., 2001. The timing of partial melting, Barrovian metamorphism and granite intrusion in the Naxos metamorphic core complex, Cyclades, Aegean Sea, Greece. *Tectonophysics* 342, 275-312.

Kretz, R., 1983. Symbols for rock-forming minerals. *American Mineralogist* 68, 277-279.

Leake, B.E., Woolley, A.R., Arps, C.E.S., Birch, W.D., Gilbert, M.C., Grice, J.D., Hawthorne, F.C., Kato, A., Kisch, H.J., Krivovichev, V.G., Linthout, K., Laird, J., Mandarino, J.A., Maresch, W.V., Nickel, E.H., Rock, N.M.S., Schumacher, J.C., Smith, D.C., Stephenson, N.C.N., Ungaretti, L., Whittaker, E.J.W., and Youshi, G., 1997. Nomenclature of amphiboles: Report of the subcommittee on amphiboles of the International Mineralogical Association, Commission on new minerals and mineral names. *American Mineralogist* 82, 1019-1037.

Li, X.H., 2000. Cretaceous magmatism and lithospheric extension in southeast China. *Journal of Asian Earth Science* 18, 293-305.

Li, J.W., Vasconcelos, P.M., Zhang, J., Zhou, M.F., Zhang, X.J., Yang, F.H., 2003. $^{40}\text{Ar}/^{39}\text{Ar}$ Constraints on a temporal link between gold mineralization, magmatism, and continental margin transtension in the Jiaodong Gold Province, eastern China. *Journal of Geology* 111, 741-751.

Li, Q.L., Chen, F., Yang, J.H., Fan, H.R., 2008. Single grain pyrite Rb-Sr dating of the Linglong gold deposit, eastern China. *Ore Geology Reviews* 34, 263-270.

Li, S., Kusky, T.M., Wang, L., Zhang, G., Lai, S., Liu, X., Dong, S., Zhao, G., 2012a. Late Mesozoic tectonic evolution of the Songliao basin, NE China: Evidence from detrital zircon ages and Sr-Nd isotopes. *Gondwana Research* 22, 943-955.

Li, S., Zhao, G., Santosh, M., Liu, X., Dai, L., Suo, Y., Tam, P.Y., Song, M., Wang, P., 2012b. Paleoproterozoic structural evolution of the southern segment of the Jiao-Liao-Ji Belt, North China Craton. *Precambrian Research* 200-203, 59-73.

Lin, W., Faure, M., Monié, P., Schärer, U., Zhang, L., Sun, Y., 2000. Tectonics of SE China, new insights from the Lushan massif (Jiangxi Province). *Tectonics* 19, 852-871.

Lin, W., Chen, Y., Faure, M., Wang, Q., 2003. Tectonic implications of new Late Cretaceous paleomagnetic constraints from Eastern Liaoning Peninsula, NE China. *Journal of Geophysical Research* 108, doi:10.1029/2002JB002169.

Lin, W., Wang, Q., 2006. Late Mesozoic extensional tectonics in the North China Block: a crustal response to subcontinental mantle removal? *Bulletin de la Société Géologique de France* 177, 287-294.

Lin, W., Faure, M., Monié, P., Wang, Q.C., 2007. Polyphase Mesozoic tectonics in the eastern part of the North China Blocks: insights from the Liaoning Peninsula massif (NE China). In: *Mesozoic sub-continental lithospheric thinning under eastern Asia* (Zhai, M.-G., Windley, B.F., Kusky, T.M., Meng, Q.R., eds). Geological Society of London, Special Publications 280, 153-170.

Lin, W., Faure, M., Monié, P., Schärer, U., Panis, D., 2008. Mesozoic extensional tectonics in Eastern Asia: The South Liaodong Peninsula Metamorphic Core Complex (NE China). *Journal of Geology* 116, 134-154.

Lin, W., Monié, P., Faure, M., Schärer, U., Shi, Y., Le Breton, N., Wang, Q., 2011. Cooling paths of the NE China crust during the Mesozoic Extensional Tectonics: example from the South Liaodong Peninsula Metamorphic Core Complex. *Journal of Asian Earth Sciences* 42, 1048-1065.

Lin, W., Faure, M., Chen, Y., Ji, W., Wang, F., Wu, L., Charles, N., Wang, Q., 2012. Late Mesozoic compressional to extensional tectonics in Yiwulüshan massif, NE China and their

bearing on Yinshan-Yanshan orogenic belt. Part I: Structural and geochronological analyses. Gondwana Research (in press). doi: 10.1016/j.gr.2012.02.013.

Lister, G.S., Banga, G., Feenstra, A, 1984. Metamorphic core complexes of Cordilleran type in Cyclades, Aegean Sea, Greece. *Geology* 12, 221-225.

Lister, G.S., Davis, G.A., 1989. The origin of metamorphic core complexes and detachments faults formed during Tertiary continental extension in the northern Colorado River region, USA. *Journal of Structural Geology* 11, 65-94.

Liu, H.F., 1986. Geodynamic scenario and structural styles of Mesozoic and Cenozoic basins in China. *American Association of Petrology and Geology Bulletin* 70, 377-395.

Liu, J., Davis, G., Lin, Z., Wu, F., 2005. The Liaonan metamorphic core complex, southeastern Liaoning Province, North China: A likely contributor to Cretaceous rotation of eastern Liaoning, Korea and contiguous areas. *Tectonophysics* 407, 65-80.

Logatchev, N.A., Zorin, Y.A., 1987. Evidence and causes for the two-stage development of the Baikal rift. *Tectonophysics* 143, 225-234.

Lorençak, M., Seward, D., Vanderhaeghe, O., Teyssier, C., Burg, J. P., 2001. Low-temperature cooling history of the Shuswap metamorphic core complex, British Columbia: constraints from apatite and zircon fission-track ages. *Canadian Journal of Earth Sciences* 38, 1615-1625.

Lynch, H.D., Morgan, P., 1987. The tensile strength of the lithosphere and the localisation of extension. In: Coward, M.P., Dewey, J.F., Hancock, P.L. (eds), Continental extensional tectonics. Geological Society Special Publications 28, 53-65.

Maruyama, S., Isozaki, Y., Kimura, G., Terabayashi, M., 1997. Paleogeographic maps of the Japanese Islands: Plate tectonic synthesis from 750 Ma to present. *Island Arc* 6, 121-142.

Mattauer, M., Matte, P., Malavieille, J., Tapponnier, P., Maluski, H., Xu, Z., Lu, Y., Tang, Y., 1985. Tectonics of Qinling belt: Build-up and evolution of eastern Asia. *Nature* 317, 496- 500.

Mazukabzov, A.M., Donskaya, T.V., Gladkochub, D.P., Sklyarov, E.V., Ponomarchuk, V.A., Sal'nikova, E.B., 2006. Structure and age of the metamorphic core complex of the Burgutui ridge (Southwestern Transbaikal region). *Dokl Earth Sci* 407, 179-183.

McDougall, I., Harrison, T.M., 1999. Geochronology and thermochronology by $^{40}\text{Ar}/^{39}\text{Ar}$ method, 2nd Ed. Oxford University Press, New York.

McGrew, A.J., Peters, M.T., Wright, J.E., 2000. Thermobarometric constraints on the tectonothermal evolution of the East Humboldt Range metamorphic core complex, Nevada. *Geol. Soc. Am.* 112, 45-60.

Meng, Q., 2003. What drove late Mesozoic extension of the northern China-Mongolia tract? *Tectonophysics* 369, 155-174.

Menzies, M.A., Fan, W.M. and Zhang, M., 1993. Palaeozoic and Cenozoic lithoprobes and the loss of >120 km of Archean lithosphere, Sino-Korean Craton, China. In: Magmatic processes and plate tectonics (Prichard, H.M., Alabaster, T., Harris, N.B.W. and Neary, C.R., eds). Geological Society of London Special Publications 76, 71-81.

Menzies, M.A., Xu, Y., Zhang, H. and Fan, W., 2007. Integration of geology, geophysics and geochemistry: A key to understanding the North China Craton. *Lithos* 96, 1-21.

Miao, S., Li, Y., Tan, W., Ren, F., 2012. Relation between the in-situ stress field and geological tectonics of a gold mine area in Jiaodong Peninsula, China. *International Journal of Rock Mechanics and Mining Sciences* 51, 76-80.

Miller, E. L., Gans, P. B., Wright, J. E., 1988. Metamorphic history of the east-central Basin and Range province: Tectonic setting and relationship to magmatism In: *Metamorphism and crustal evolution of the western United States* (Ernst, W. G., ed.). Englewood Cliffs, New Jersey Prentice-Hall Inc., 650-682.

Norlander, B.H., Whitney, D.L., Teyssier, C., Vanderhaeghe, O., 2002. Partial melting and decompression of the Thor-Odin dome, Shuswap metamorphic core complex, Canadian Cordillera. *Lithos* 61, 103-125.

Okada, H., 1999. Plume-related sedimentary basins in East Asia during the Cretaceous. *Palaeogeography Palaeoclimatology Palaeoecology* 150, 1-11.

Péron-Pinvidic, G., Van Wijk, J., Shillington, D.J., Gerginon, L., (Eds) 2009. Role of magmatism in continental lithosphere extension. *Tectonophysics* 468.

Ren, J., Tamaki, K., Li, S. and Junxia, Z., 2002. Late Mesozoic and Cenozoic rifting and its dynamic setting in Eastern China and adjacent areas. *Tectonophysics* 344, 175-205.

Rey, P.F., Teysier, C., Whitney, D.L., 2009a. Extension rates, crustal melting, and core complex dynamics. *Geology* 37, 391-394.

Rey, P.F., Teysier, C., Whitney, D.L., 2009b. The role of partial melting and extensional strain rates in the development of metamorphic core complexes. *Tectonophysics* 477, 135-144.

Reynolds, S.J., Rehrig, W.A., 1980. Mid-Tertiary plutonism and mylonitisation, South Mountains, central Arizona. In: Crittenden, M.C., Coney, J.P., Davis, G.H. (eds), *Cordilleran metamorphic core complexes*. Geological Society of America Memoir, Boulder, 159-175.

Ring, U., Johnson, C., Hetzel, R., Gessner, K., 2003. Tectonic denudation of a Late Cretaceous-Tertiary collisional belt: regionally symmetric cooling patterns and their relation to extensional faults in the Anatolide belt of western Turkey. *Geol. Mag.* 140, 421-441.

Ring, U., Collins, A.S., 2005. SHRIMP dating of the syn-tectonic Egrigöz granite: Precise timing of core-complex formation in the Anatolide belt of western Turkey. *Journal of Geological Society, London* 162, 289-298.

Rosenbaum, G., Weinberg, R.F., Regenauer-Lieb, K., 2008. The geodynamics of lithospheric extension. *Tectonophysics* 458, 1-8.

Samson, S.D., Alexander, E.C., 1987. Calibration of the interlaboratory $^{40}\text{Ar}/^{39}\text{Ar}$ dating standard, MMhb-1. *Chemical Geology* 66, 27-34.

Sang, L.K., 1984. The origin and evolution of the Linglong granites. *Earth Sciences* 9, 101-114 (in Chinese).

SBGMR, 1991. Regional geology of the Shandong Province. Geological Memoirs of Ministry of Geology and Mineral Resources, 26, Geological Publishing House, Beijing, 699 p.

Sengör, A.M., Burke, K., 1978. Relative timing of rifting and volcanism on Earth and its tectonic implications. *Geophysical Research Letters* 5, 419-421.

Sklyarov, E.V., Mazukabzov, A.M., Donskaya, T.V., Doronina, N.A., Shafeev, A.A., 1994. Metamorphic core complexes of the Zagan Range (Transbaikalia). *Dokl Earth Sciences* 339, 83-86.

Sullivan, W.A., Snoke, A.W., 2007. Comparative anatomy of core-complex development in the northeastern Great Basin, U.S.A. *Rocky Mountain Geology* 42, 1-29.

Tagami, T., Shimada, C., 1996. Natural long-term annealing of the fission-track system around a granitic pluton. *Journal of Geophysical Research* 101, 8245-8255.

Tam, P.K., Zhao, G.C., Liu, F.L., Zhou, X.W., Sun, S., Li, S.Z., 2011. Timing of metamorphism in the Paleoproterozoic Jiao-Liao-Ji Belt: new SHRIMP U-Pb zircon dating of granulites, gneisses and marbles of the Jiaobei massif in the North China Craton. *Gondwana Research* 19, 150-162.

Tam, P.Y., Zhao, G., Zhou, X., Sun, M., Guo, J., Li, S., Yin, C., Wu, M., He, Y., 2012. Metamorphic P-T path and implications of high-pressure pelitic granulites from the Jiaobei massif in the Jiao-Liao-Ji Belt, North China Craton. *Gondwana Research* 22, 104-117.

Tang, J., Zheng, Y.F., Wu, Y.B., Gong, B., Liu, X.M., 2007. Geochronology and geochemistry of metamorphic rocks in the Jiaobei terrane: constraints on its tectonic affinity in the Sulu orogen. *Precambrian Research* 152, 48-82.

Tirel, C., Brun, J.P., Sokoutis, D., 2006. Extension of thickened and hot lithospheres: Inferences from laboratory modeling. *Tectonics* 25, doi:10.1029/2005TC001804.

Tirel, C., Brun, J.P., Burov, E., 2008. Dynamics and structural development of metamorphic core complexes. *Journal of Geophysical Research* 113, B04403, <http://dx.doi.org/10.1029/2005JB003694>.

Tomassi, A., Vauchez, A., Fernandes, L.A.D., Porcher, C.C., 1994. Magma assisted strain localization in an orogen-parallel transcurrent shear zone of southern Brazil. *Tectonics* 13, 421-437.

Turrillot, P., Augier, R., Monié, P., Faure, M., 2011. Late-orogenic exhumation of the Variscan high-grade units (South Armorican Domain, Western France), combined structural and $^{40}\text{Ar}/^{39}\text{Ar}$ constraints. *Tectonics*, doi:10.1029/2010TC002788.

Vanderhaeghe, O., Teyssier, C., 1997. Formation of the Shuswap metamorphic core complex during late-orogenic collapse of the Canadian Cordillera: role of ductile thinning and partial melting of the mid- to lower crust. *Geodinamica Acta* 10, 41-58.

Vanderhaeghe, O., Teyssier, C., Wysoczanski, R., 1999. Structural and geochronologic constraints on the role of partial melting during the formation of the Shuswap metamorphic core complex at the latitude of the Thor-Odin dome, British Columbia. *Canadian Journal of Earth Sciences* 36, 917-943.

Vanderhaeghe, O., 2004. Structural development of the Naxos migmatite dome. *Geological Society of America, Special Papers* 380, 211-227.

Van der Molen, I., Paterson, M.S., 1979. Experimental deformation of partially-melted granite. *Contributions to Mineralogy and Petrology* 70, 299-318.

Villa, I.M., 1998. Isotopic closure. *Terra Nova* 10, 42-47.

Wan, T., Teyssier, C., Zeng, H., Zhou, W., Tikoff, B., 2001. Emplacement mechanism of Linglong granitoid complex, Shandong Peninsula, China. *Science in China (Series D)* 44, 535-544.

Wang, P.C., 1995. Relationships between the Jingshan Group and the Fenzishan Group in the Jiaobei area. *Regional Geology of China* 1, 15-20 (in Chinese with English abstract).

Wang, L.G., Qiu, Y.M., McNaughton, N.J., Groves, D.I., Luo, Z.K., Huang, J.Z., Miao, L.C. and Liu, Y.K., 1998. Constraints on crustal evolution and gold metallogeny in the Northwestern Jiaodong Peninsula, China, from SHRIMP U-Pb zircon studies of granitoids. *Ore Geology Reviews* 13, 275-291.

Wang, F., Zhou X.-H., Zhang, L.-C., Ying, J.-F., Zhang, Y.-T., Wu, F.-Y., Zhu, R.-X., 2006. Late Mesozoic volcanism in the Great Xing'an Range (NE China): Timing and implications for the dynamic setting of NE Asia. *Earth and Planetary Science Letters* 251, 179-198.

Watson, M.P., Hayward, A.B., Parkinson, D.N., Zhang, Z.M., 1987. Plate tectonic history, basin development and petroleum source rock deposition onshore China. *Marine Petroleum Geology* 4, 205-225.

Wawrzenitz, N., Krohe, A., 1998. Exhumation and doming of the Thasos metamorphic core complex (S Rhodope, Greece): structural and geochronological constraints. *Tectonophysics* 285, 301-332.

Webb, L.E., Graham, S.A., Johnson, C.L., Badarch, G. and Hendrix, S., 1999. Occurrence, age, and implications of the Yagan-Onch Hayrhan metamorphic core complex, southern Mongolia. *Geology* 27, 143-146.

Weingartner, H., Hejl, E., 1994. The relief generations of Thassos and the first attempt of fission-track dating in the Northern Greece. *Bulletin of Geological Society of Greece* 30, 307-312.

Wu, F.Y., Sun, D.Y., 1999. Mesozoic magmatism and lithospheric thinning in eastern China. *Journal of Changchun Science and Technology University* 29, 313-318 (in Chinese).

Wu, F.Y., Jahn, B.M., Wilde, S., Sun, D.Y., 2000. Phanerozoic crustal growth: U-Pb and Sr-Nd isotopic evidence from the granites in northeastern China. *Tectonophysics* 328, 89-113.

Wu, F.Y., Lin, J.Q., Wilde, S.A., Zhang, X.O., Yang, J.H., 2005a. Nature and significance of the Early Cretaceous giant igneous event in eastern China. *Earth and Planetary Sciences Letters* 233, 103-119.

Wu, F.Y., Yang, J.H., Wilde, S.A., Zhang, X.O., 2005b. Geochronology, petrogenesis and tectonic implications of Jurassic granites in the Liaodong Peninsula, NE China. *Chemical Geology* 221, 127-156.

Wu, F.Y., Han, R.H., Yang, J.H., Wilde, S.A., Zhai, M.G., Park, S.C., 2007. Initial constraints on the timing of granitic magmatism in North Korea using U-Pb zircon geochronology. *Chemical Geology* 238, 232-248.

Yang, J.H., Wu, F.Y., Wilde, S.A., 2003. A review of the geodynamic setting of large-scale Late Mesozoic gold mineralization in the North China Craton: an association with lithospheric thinning. *Ore Geology Reviews* 23, 125-152.

Yang, J.H., Wu, F.Y., Chung, S.L., Lo, C.H., Wilde, S.A., Davis, G.A., 2007. Rapid exhumation and cooling of the Liaonan metamorphic core complex: Inferences from $^{40}\text{Ar}/^{39}\text{Ar}$ thermochronology and implications for Late Mesozoic extension in the eastern North China Craton. *Geological Society of America Bulletin* 119, 1405-1414.

Yang, J.H., Wu, F.Y., Chung, S.L., Lo, C.H., 2008. The extensional geodynamic setting of Early Cretaceous granitic intrusions in the eastern North China Craton: Evidence from laser $^{40}\text{Ar}/^{39}\text{Ar}$ dating of K-bearing minerals. *Acta Petrologica Sinica* 24, 1175-1184.

Yang, K.F., Fan, H.R., Santosh, M., Hu, F.F., Wilde, S.A., Lan, T.G., Lu, L.N., Liu, Y.S., 2012. Reactivation of the Archean lower crust: Implications for zircon geochronology, elemental and Sr-Nd-Hf isotopic geochemistry of late Mesozoic granitoids from northwestern Jiaodong Terrane, the North China Craton. *Lithos* 146-147, 112-127.

Yin, A., Nie, S., 1996. A Phanerozoic palinspastic reconstruction of China and its neighboring regions. In: Yin, A., and Harrison, T.A. (eds). *The tectonic evolution of Asia*. New York, Cambridge University Press, 442-485.

Zhai, M.G., Windley, B.F., Kusky, T.M., Meng, Q.R. (eds), 2007. Mesozoic sub-continental lithospheric thinning under eastern Asia. *Geological Society, London, Special Publications* 280.

Zhai, M.G., Santosh, M., 2011. The early Precambrian odyssey of the North China Craton: A synoptic overview. *Gondwana Research* 20, 6-25.

Zhang, X., Cawood, P.A., Wilde, S.A., Liu, R., Song, H., Li, W., Snee, L.W., 2003. Geology and timing of mineralization at the Cangshang gold deposit, northwestern Jiaodong Peninsula, China. *Mineralium Deposita* 38, 141-153.

Zhang, H.Y., Hou, Q.L., Cao, D.Y., 2007. Tectono-chronologic constraints on a Mesozoic slip and thrust belt in the eastern Jiaodong Peninsula. *Science in China Series D* 50, 25-32.

Zhang, R.Y., Liou, J.G., Ernst, W.G., 2009. The Dabie-Sulu continental collision zone: A comprehensive review. *Gondwana Research* 16, 1-26.

Zhang, J.H., Gao, S., Ge, W.C., Wu, F.Y., Yang, J.H., Wilde, S.A., Li, M., 2010a. Geochronology of the Mesozoic volcanic rocks in the Great Xing'an Range, northeastern China: Implications for subduction-induced delamination. *Chemical Geology* 276, 144-165.

Zhang, J., Zhao, Z.F., Zheng, Y.F., Dai, M., 2010b. Postcollisional magmatism: Geochemical constraints on the petrogenesis of Mesozoic granitoids in the Sulu orogen, China. *Lithos* 119, 512-536.

Zhang, F.Q., Chen, H.L., Yu, X., Dong, C.W., Yang, S.F., Pang, Y.M., Batt, G.E., 2011. Early Cretaceous volcanism in the northern Songliao basin, NE China, and its geodynamic implication. *Gondwana Research* 19, 163-176.

Zhao, G.C., Sun, M., Wilde, S.A., Li, S.Z., 2005. Late Archean to Paleoproterozoic evolution of the North China Craton: key issues revisited. *Precambrian Research* 136, 177-202.

Zhao, L., Zheng, T.Y., Chen, L., Tang, Q.S., 2007. Shear wave splitting in eastern and Central China: implications for upper mantle deformation beneath continental margin. *Physics of the Earth and Planetary Interiors* 162, 73-84.

Zhou, T., Lü, G., 2000. Tectonics, granitoids and Mesozoic gold deposits in East Shandong, China. *Ore Geology Reviews* 16, 71-90.

Zhou, J.B., Wilde, S.A., Zhao, G.C., Zheng, C.Q., Jin, W., Zhang, X.Z., Cheng, H., 2008. SHRIMP U-Pb zircon dating of the Neoproterozoic Penglai Group and Archean gneisses from the Jiaobei Terrane, North China Craton, and their tectonic implications. *Precambrian Research* 160, 323-340.

Figure captions

Fig. 1. Review geological map of East Asia. Represented are the main presumed late Mesozoic and Cenozoic extensional markers including sedimentary basins, magmatic rocks and extensional domes and MCCs with the kinematics of the detachments faults and intracrustal shear zones. See Lin and Wang (2006) and Charles (2010) for references. Abbreviations for domes and MCCs: BU = Buteel-Burgutoy; ED = Ereendavaa; ER = Ertomia; GD = Gudaoling; HG = Hongzhen ; KA = Kalaqin; LL = Linglong; LS =Lushan; LU = Luotian; SL = Sud Liaodong; XI = Xishan; YA =Yagan- Onch Hayrhan; YW = Yiwulüshan ; ZA = Zagan. Tan-Lu F. = Tan-Lu fault; NCC = North China Craton; SCC = South China Craton.

Fig. 2. (a) Simplified geological map of Jiaodong Peninsula (Shandong Province) showing the importance of late Mesozoic tectonics and magmatic activity. GJL = Guojialing synkinematic pluton; LDF = Linglong detachment fault; GSZ = Guojialing shear zone. Isotropic plutons are represented by pinkish-reddish granodiorite (PRG) plutons intruded throughout the Jiaodong Peninsula. (b) Detailed geological map of Linglong MCC (LL) exhumed below the Linglong detachment fault (LDF), cross-cut to the north by the Guojialing pluton (GJL) emplaced below the Guojialing intracrustal extensional shear zone (GSZ). Are shown both magnetic lineations (Wan et al., 2001, Charles, 2010) and stretching lineation and associated sense of shear measured in the field (Charles et al., 2011a). Indicated are available time-constraints (Wang et al., 1998). Note the small PRG plutons intruded into the Linglong MCC. Stereograms are projected within the lower hemisphere.

Fig. 3. Main results of the mineral chemical compositions and their representative habits. (a) to (d): Representative textures of dated minerals. (a) Inherited magmatic white-mica clasts strongly deformed within a mylonite sample (Sample 165-08). (b) Newly-crystallised white-micas on a brittle fault-plane (Sample 91-07). Note also the presence of white-mica growth into the host-rock. (c) and (d): Representative microphotographs of amphibole and biotite grains from the isotropic Guojialing granodiorite (Sample 167-08), respectively. Similar textures are encountered in samples from the PRG plutons. (e) Variation of X_{Mg} vs. Si^{IV} contents in white-micas. (f) $Mg/(Mg+Fe^{2+})$ vs. Si^{IV} classification for calcic amphiboles (Leake et al., 1997). (g) Al^{IV} vs. $(Fe/Fe+Mg)$ classification for biotites. Abbreviations: qz (quartz), bt (biotite), am (amphibole), kfs (K-feldspar), Wm (white mica).

Fig. 4. Synthesis of the conventional $^{40}Ar/^{39}Ar$ results presented as age spectra (a to e). Are also provided thermochronologic paths for the Linglong MCC (f), Guojialing pluton and

isotropic PRG pluton (g). Mean mineral closure temperatures are from McDougall and Harrison (1999); closure temperature interval is routinely around $\pm 50^{\circ}\text{C}$. 1σ uncertainties for all graphs, sample locations in Figure 2b and analytical details in Table 2. Mineral abbreviations are after Kretz (1983).

Fig. 5. Diachronism between the main magmatism pulses and crustal extensional strain amount in East Asia as viewed by the compilation of timing for MCC development, magmatic rocks emplacement and extensional sedimentary basin infilling (i.e. tectonic subsidence). Are also displayed the emplacement ages of representative isotropic plutons. Abbreviations: YOH = Yagan-Onch Hayrhan (Webb et al., 1999); YW = Yiwulüshan (Darby et al., 2004); ER = Ereendavaa (Daoudene et al., 2009, 2011); SL = South Liaodong (Yang et al., 2007; Lin et al., 2011); GD = Gudaoling and YMW = Yinmawanshan (Charles, 2010; Charles et al., 2012); LAO = Laohushan (Lin et al., 2007); LJ = Luanjiahe (Wang et al., 1998); NAR = Nartyn (Daoudene et al., 2011); AI = Aishan (SBGMR, 1991); BA = Badaling (BBGMR, 1991); HY = Haiyang (Charles et al., 2011b); XUE = Xuejiashiliang and DA = Dahaituo (Davis et al., 2001); WD = Weideshan (Zhang et al., 2007). Relative emplacement age probability is after Wu et al. (2005b). See Ren et al., (2002); Meng (2003); Li et al. (2012) for sedimentary basins data. *corresponds to age-data from this study.

Fig. 6. Compilation of radiochronological data constraining the complete duration for the MCC development throughout different extensional domains of the world. The onset of the tectonic evolution is marked by the crystallisation age of migmatites and/or the associated granites using, mostly, U/Pb ages on zircon. Data from the Basin & Range and the Aegean regions (Miller et al., 1988; Vanderhaeghe et al. 1997; Wawrzenitz and Krohe 1998; Vanderhaeghe et al. 1999; McGrew et al. 2000; Keay et al. 2001; Lorencak et al. 2001;

Norlander et al., 2002; Ring et al. 2003; Isik et al. 2004; Ring and Collins, 2005; Brichau et al. 2006; Duchêne et al. 2006; Sullivan and Snoke 2007) are compared with recent time-constraints obtained from eastern China MCCs (Wang et al., 1998; Wu et al., 2005a, b; Yang et al., 2007, 2008; this study). Mean mineral closure temperatures are from Tagami and Shimada (1996); Villa (1998) and Harrisson et al. (2009); closure temperature interval is routinely around $\pm 30-50^{\circ}\text{C}$.

Tables

Table 1: Summary of conventional $^{40}\text{Ar}/^{39}\text{Ar}$ results. For each conventional analysis, both the total gas age and the inverse isochrone age are given with the corresponding statistical parameters. TFA = Total Fusion Age; IIA = Inverse Isochron Age; PA = Plateau Age (segment). Mineral abbreviations are after Kretz (1983): ms = muscovite; am = amphibole; bt = biotite. LDF = Linglong detachment fault; GSZ = Guojialing shear zone; PRG = pinkish-reddish granodiorite pluton.

Table 2: Complete results of conventional $^{40}\text{Ar}/^{39}\text{Ar}$ analyses. Reported are the J factor, isotopic ratios and apparent calculated ages in Ma with the corresponding errors (1σ).

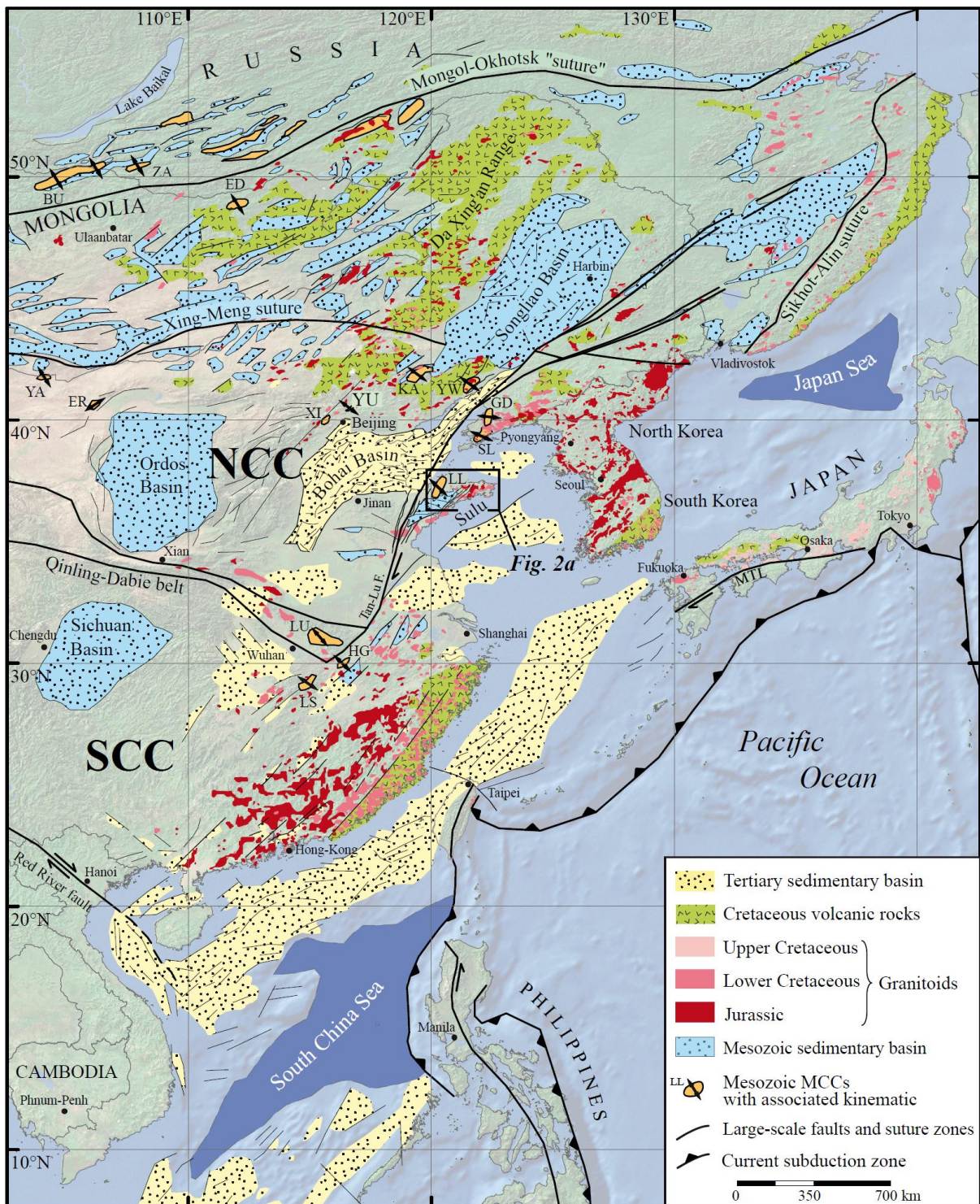


Figure 1

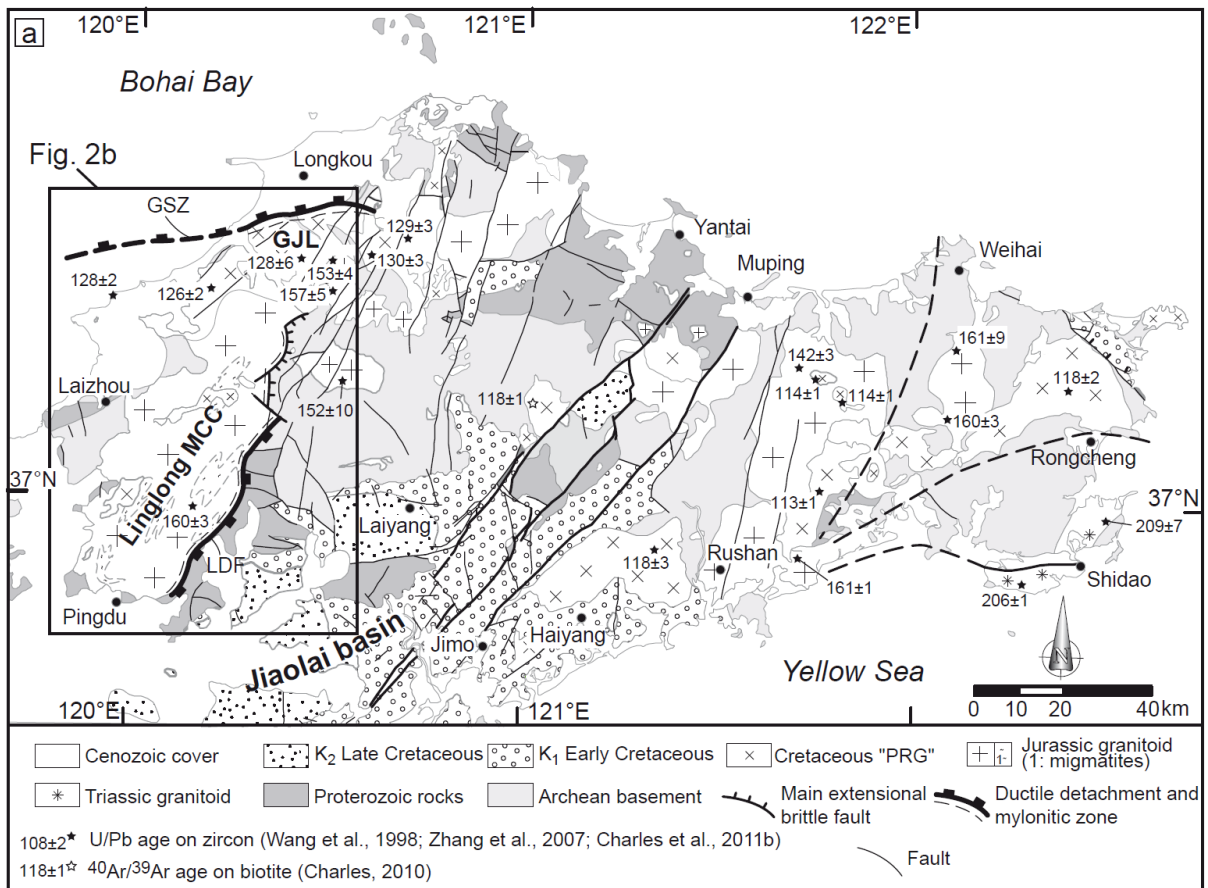


Figure 2a

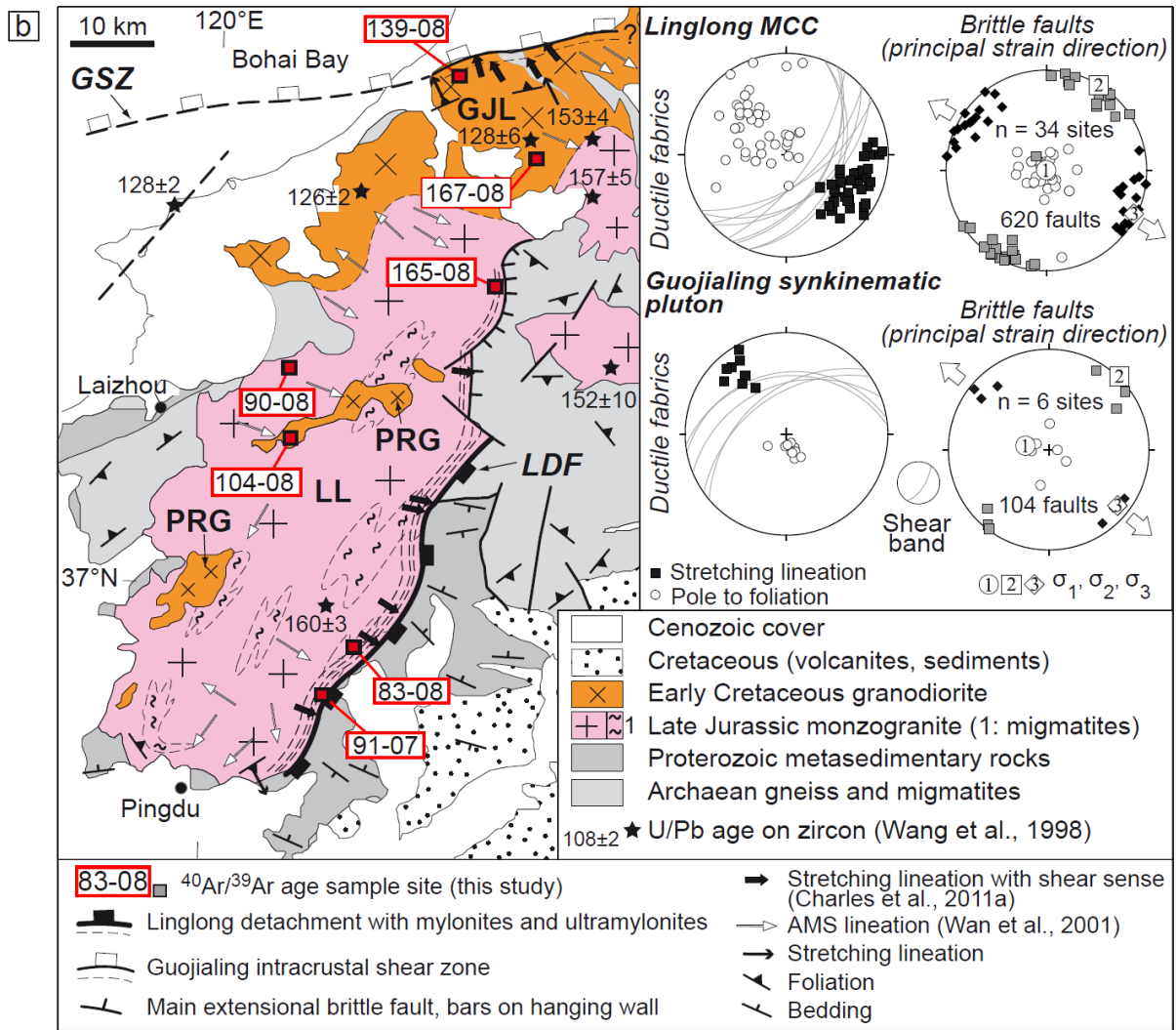


Figure 2b

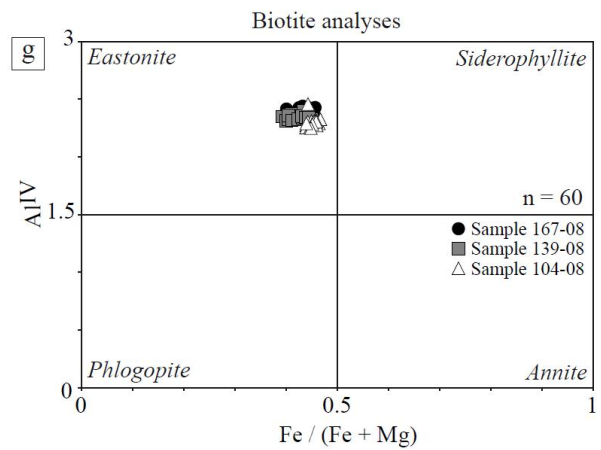
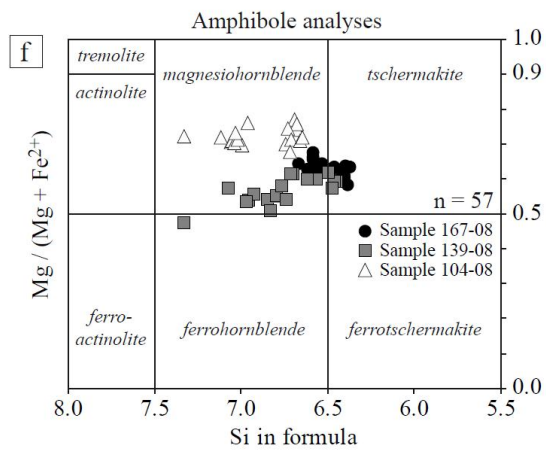
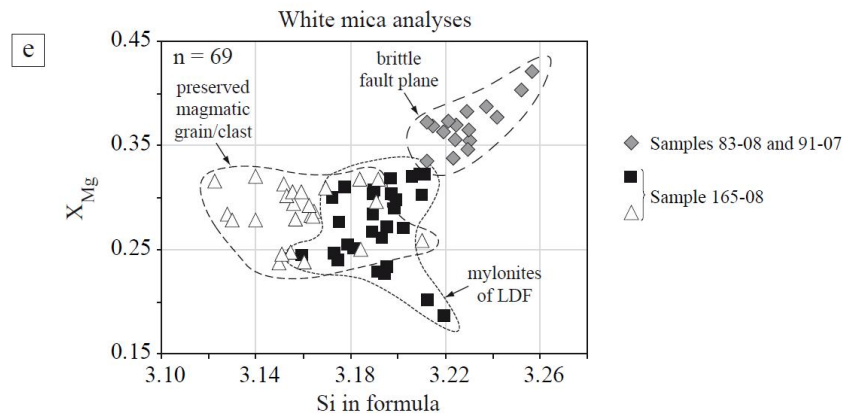
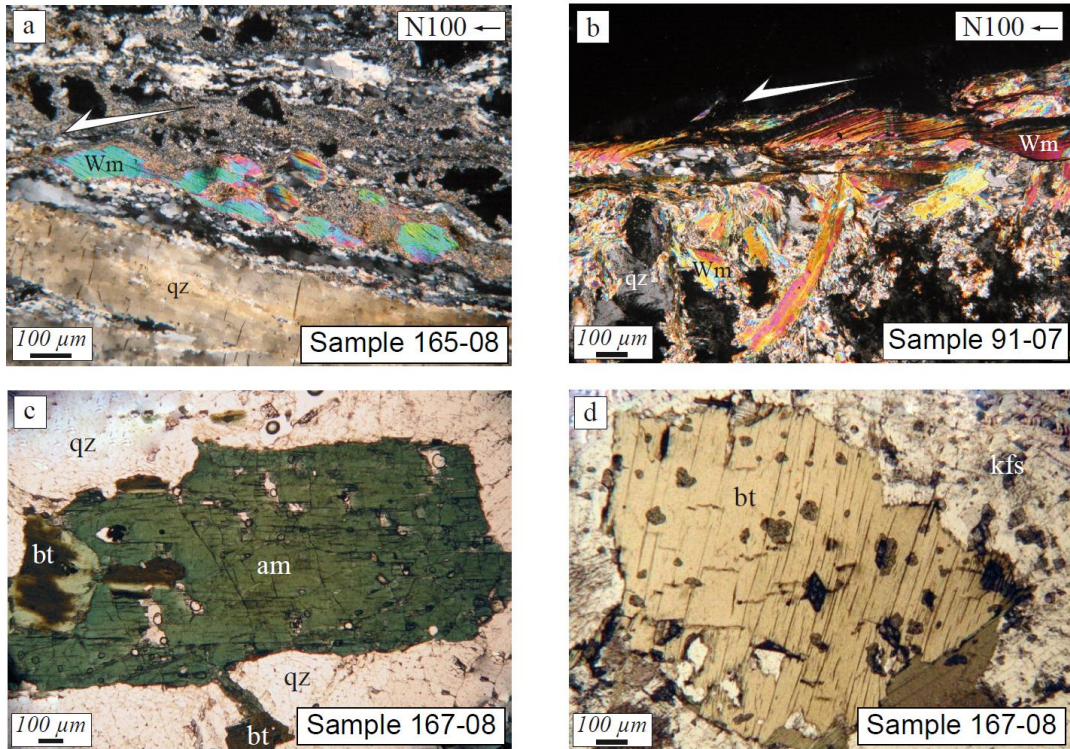


Figure 3

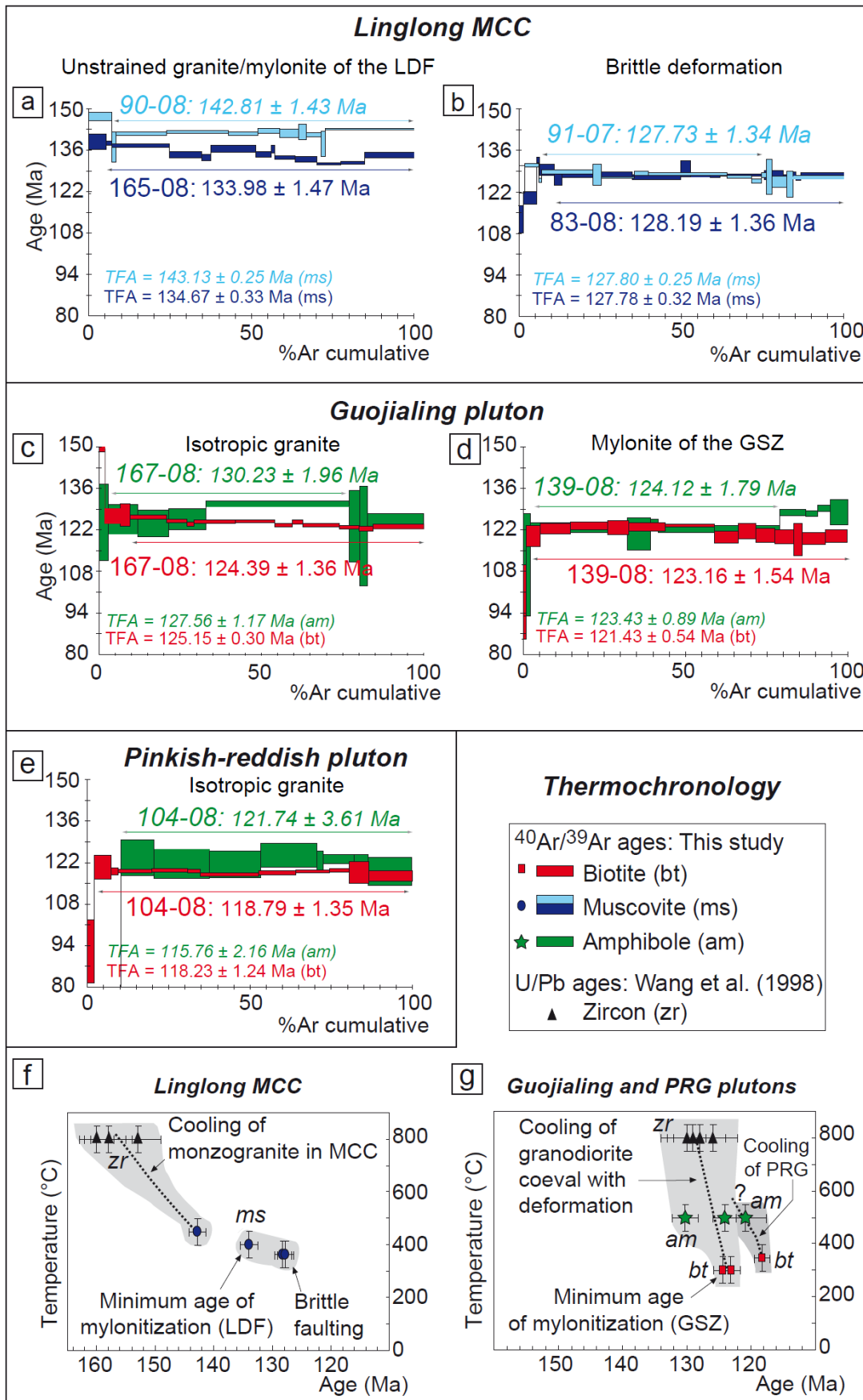
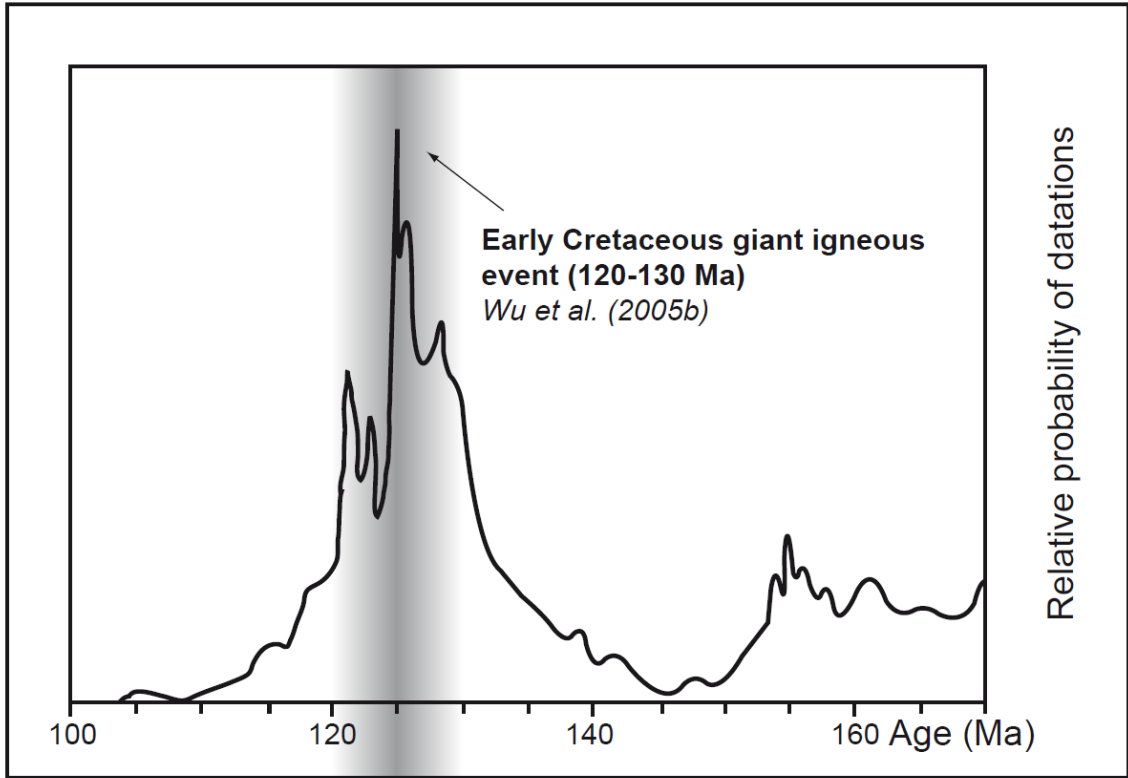


Figure 4

a



b

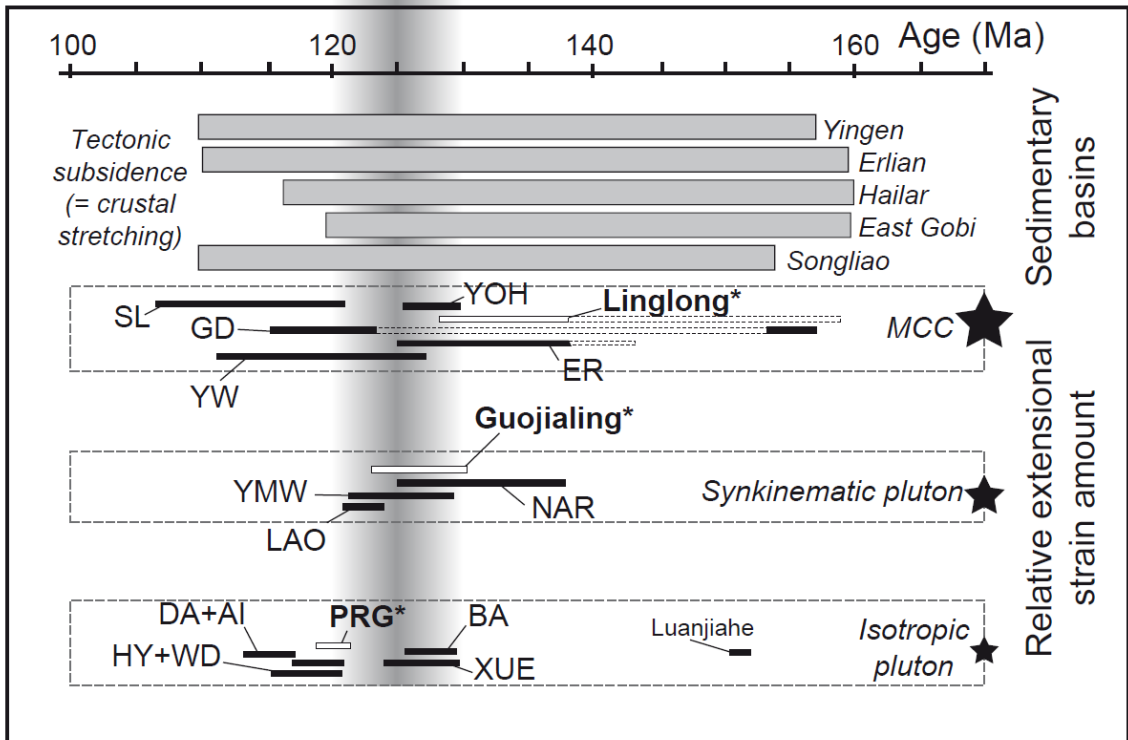


Figure 5

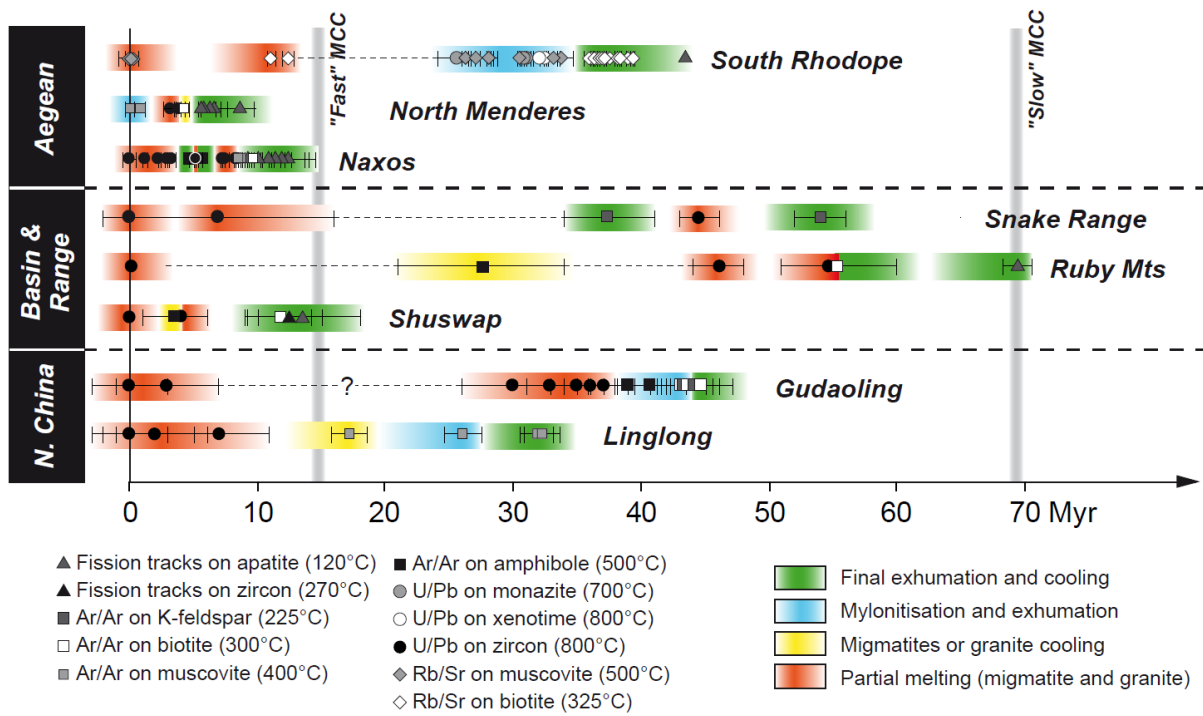


Figure 6

Sample number	Long (°E); Lat (°N)	Rock type	Mineral	TFA (Ma)	IIA (Ma)	PA (Ma)
90-08	120.085; 37.227	isotropic monzogranite	ms	143.13±0.25	142.11±1.41	142.81±1.43
165-08	120.388; 37.330	mylonite of LDF	ms	134.67±0.33	134.18±1.45	133.98±1.47
91-07	120.162; 36.881	brittle fault plane of LDF	ms	127.80±1.27	127.84±1.32	127.73±1.34
83-08	120.211; 36.928	brittle fault plane of LDF	ms	127.78±0.32	128.50±1.37	128.19±1.36
167-08	120.419; 37.464	isotropic GJL	am	127.56±1.17	129.88±2.03	130.23±1.96
		isotropic GJL	bt	125.15±0.30	124.42±1.24	124.39±1.36
139-08	120.325; 37.560	mylonite of GSZ	am	123.43±0.89	125.87±1.44	124.12±1.79
		mylonite of GSZ	bt	121.43±0.54	122.25±1.32	123.16±1.54
104-08	120.111; 37.163	isotropic PRG	am	115.76±2.16	121.71±1.32	121.74±3.61
		isotropic PRG	bt	118.23±1.24	119.15±1.17	118.79±1.35

Table 1

Step	$^{40}\text{Ar}/^{39}\text{Ar}$	$^{38}\text{Ar}/^{39}\text{Ar}$	$^{37}\text{Ar}/^{39}\text{Ar}$	$^{36}\text{Ar}/^{39}\text{Ar}$ (e-3)	^{39}Ar (e-14)	% ^{39}Ar	% $^{40}\text{Ar}^*$	$^{40}\text{Ar}^*/^{39}\text{K}$	Age (Ma)	Error
<i>J= 0.00717 for all samples</i>										
90-08_ms (Fig. 4a)										
1	15.595	0.016	0.00606	12.567	0.279	7.12	76.09	11.87	147.31	1.42
2	11.742	0.012	0.00000	2.443	0.055	8.34	93.72	11.00	137.01	5.08
3	11.546	0.013	0.00000	0.475	0.704	23.83	98.65	11.39	141.62	0.57
4	11.462	0.016	0.00270	0.063	0.871	43.01	99.70	11.43	142.09	0.51
5	11.393	0.013	0.00316	0.000	0.407	51.97	99.86	11.38	141.47	0.59
6	11.480	0.013	0.00874	0.000	0.310	58.79	99.86	11.47	142.53	0.75
7	11.410	0.012	0.00000	0.000	0.263	64.59	99.86	11.39	141.68	1.31
8	11.550	0.012	0.00000	0.330	0.104	66.87	99.02	11.44	142.19	2.61
9	11.376	0.012	0.00000	0.000	0.209	71.48	99.86	11.36	141.27	0.68
10	11.502	0.013	0.00000	1.329	0.061	72.82	96.45	11.09	138.07	4.22
11	11.536	0.013	0.00025	0.000	1.235	100.00	99.86	11.52	143.19	0.26
165-08_ms (Fig. 4a)										
1	13.710	0.016	0.00487	8.696	0.109	5.35	81.15	11.13	138.46	2.55
2	11.100	0.012	0.00000	0.000	0.037	7.00	99.86	11.08	137.96	0.79
3	11.029	0.013	0.00000	0.000	0.397	24.70	99.86	11.01	137.12	0.54
4	10.778	0.013	0.00000	0.000	0.224	34.67	99.86	10.76	134.10	1.00
5	10.695	0.017	0.01770	0.000	0.062	37.45	99.85	10.68	133.13	1.09
6	10.943	0.013	0.00000	0.000	0.312	51.36	99.86	10.93	136.09	1.18
7	10.788	0.013	0.00858	0.000	0.104	55.98	99.86	10.77	134.23	0.89
8	10.928	0.019	0.04513	0.000	0.025	57.11	99.86	10.92	135.95	1.27
9	10.697	0.013	0.00673	0.000	0.143	63.47	99.85	10.68	133.14	0.56
10	10.641	0.013	0.00061	0.000	0.146	70.01	99.85	10.63	132.46	0.90
11	10.517	0.013	0.00027	0.000	0.166	77.40	99.85	10.50	130.97	0.45
12	10.544	0.013	0.00194	0.000	0.166	84.79	99.85	10.53	131.29	0.49
13	10.756	0.013	0.00000	0.005	0.341	100.00	99.84	10.74	133.82	0.94
91-07_ms (Fig. 4b)										
1	13.379	0.019	0.00000	10.960	0.060	2.03	75.68	10.12	126.43	4.61
2	10.541	0.013	0.00000	0.000	0.121	6.16	99.85	10.53	131.26	0.55
3	10.108	0.011	0.00000	0.000	0.029	7.16	99.85	10.09	126.04	0.79
4	10.341	0.013	0.00000	0.000	0.462	22.90	99.85	10.33	128.85	0.72
5	10.274	0.012	0.00000	0.003	0.076	25.50	99.84	10.26	128.03	3.60
6	10.187	0.013	0.00000	0.000	0.297	35.62	99.85	10.17	127.00	0.32
7	10.304	0.013	0.00000	0.000	0.126	39.92	99.85	10.29	128.40	0.72
8	10.293	0.013	0.00000	0.000	0.713	64.23	99.85	10.28	128.27	0.47
9	10.206	0.012	0.00122	0.000	0.217	71.64	99.85	10.19	127.22	0.55
10	10.089	0.013	0.01141	0.000	0.088	74.65	99.85	10.07	125.82	0.68
11	10.250	0.014	0.06262	0.000	0.050	76.34	99.85	10.24	127.81	0.85
12	10.281	0.011	0.02613	0.260	0.046	77.91	99.12	10.19	127.22	5.99
13	10.154	0.013	0.00376	0.278	0.137	82.56	99.04	10.06	125.60	1.97
14	10.147	0.011	0.00000	0.506	0.059	84.57	98.37	9.98	124.71	4.40
15	10.186	0.013	0.00444	0.000	0.453	100.00	99.85	10.17	126.99	0.50
83-08_ms (Fig. 4b)										
1	12.478	0.018	0.11312	11.625	0.048	1.47	72.41	9.04	113.26	4.57
2	10.702	0.014	0.05257	3.594	0.135	5.56	89.97	9.63	120.44	2.05
3	10.695	0.014	0.09210	0.000	0.028	6.42	99.85	10.69	133.20	0.92
4	10.867	0.013	0.04099	1.461	0.151	11.00	95.91	10.42	130.02	1.88
5	10.145	0.013	0.13502	0.000	0.076	13.32	99.85	10.14	126.63	1.89
6	10.482	0.013	0.00375	0.653	0.713	34.96	98.01	10.27	128.23	0.95
7	10.343	0.012	0.00415	0.392	0.490	49.84	98.73	10.21	127.48	0.89
8	10.482	0.011	0.01536	0.100	0.104	53.01	99.58	10.44	130.21	2.74
9	10.279	0.013	0.00000	0.000	0.199	59.06	99.85	10.26	128.10	0.54
10	10.287	0.012	0.02885	0.000	0.097	62.01	99.85	10.27	128.23	0.80
11	10.281	0.012	0.00000	0.000	0.451	75.70	99.85	10.27	128.12	0.29

12	10.326	0.012	0.00000	0.155	0.188	81.40	99.40	10.26	128.12	1.50
13	10.229	0.015	0.06232	0.000	0.088	84.08	99.85	10.22	127.56	0.74
14	10.274	0.015	0.01695	0.000	0.038	85.22	99.85	10.26	128.06	1.19
15	10.206	0.012	0.00000	0.000	0.056	86.93	99.85	10.19	127.23	0.77
16	10.317	0.012	0.00000	0.000	0.430	100.00	99.85	10.30	128.56	0.39
167-08_am (Fig. 4c)										
1	14.576	0.214	0.62944	15.725	0.018	2.89	68.34	9.96	124.50	12.97
2	14.366	0.269	1.43559	14.895	0.057	11.99	70.00	10.07	125.72	4.97
3	12.016	0.268	1.30006	7.343	0.059	21.40	82.62	9.94	124.15	4.50
4	11.458	0.260	1.19258	5.026	0.072	32.94	87.68	10.05	125.58	3.51
5	11.163	0.259	0.17370	2.267	0.277	77.02	93.98	10.49	130.85	1.06
6	10.629	0.253	1.40939	2.911	0.020	80.27	92.75	9.87	123.32	12.07
7	10.477	0.262	0.13527	3.002	0.014	82.56	91.48	9.59	119.92	16.92
8	10.917	0.245	1.24108	3.308	0.110	100.00	91.76	10.03	125.23	2.37
167-08_bt (Fig. 4c)										
1	33.926	0.061	0.10798	72.384	0.047	2.13	36.93	12.53	155.21	6.92
2	10.732	0.042	0.00612	1.921	0.105	6.86	94.57	10.15	126.72	2.48
3	10.311	0.045	0.03413	0.423	0.068	9.92	98.66	10.17	127.02	3.80
4	10.126	0.043	0.00714	0.000	0.247	21.01	99.85	10.11	126.27	0.71
5	10.020	0.043	0.03670	0.000	0.143	27.41	99.84	10.01	125.01	0.55
6	9.930	0.047	0.02631	0.000	0.046	29.50	99.84	9.92	123.91	0.75
7	9.998	0.043	0.00971	0.000	0.284	42.23	99.84	9.98	124.72	0.60
8	10.008	0.043	0.00762	0.000	0.271	54.41	99.84	9.99	124.84	0.43
9	9.900	0.041	0.01239	0.000	0.118	59.70	99.84	9.89	123.55	0.55
10	9.999	0.042	0.01472	0.000	0.075	63.07	99.84	9.98	124.73	0.69
11	9.903	0.042	0.00608	0.000	0.249	74.27	99.84	9.89	123.57	0.65
12	9.843	0.042	0.00212	0.000	0.133	80.22	99.84	9.83	122.84	0.63
13	9.807	0.041	0.03605	0.000	0.096	84.54	99.84	9.79	122.44	0.90
14	9.867	0.042	0.00580	0.000	0.344	100.00	99.84	9.85	123.13	0.79
139-08_am (Fig. 4d)										
1	16.341	0.085	0.00000	25.495	0.011	2.19	53.80	8.79	110.28	17.28
2	12.680	0.124	0.04880	9.606	0.149	32.02	77.52	9.83	122.87	1.68
3	10.425	0.118	0.07667	2.587	0.036	39.24	92.57	9.65	120.71	5.46
4	9.984	0.107	0.00000	0.000	0.011	41.51	99.84	9.97	124.55	1.13
5	10.366	0.127	0.00724	1.933	0.186	78.92	94.35	9.78	122.26	1.15
6	10.110	0.139	1.85464	0.000	0.040	86.99	99.85	10.25	127.89	0.96
7	10.210	0.125	0.28968	0.000	0.019	90.72	99.85	10.22	127.55	1.01
8	10.210	0.125	2.08800	0.000	0.019	94.44	99.85	10.36	129.32	1.01
9	10.379	0.119	2.10523	0.925	0.028	100.00	98.74	10.26	128.08	4.28
139-08_bt (Fig. 4d)										
1	14.378	0.035	0.01391	22.353	0.021	1.23	53.96	7.76	97.66	12.56
2	12.107	0.023	0.00000	8.462	0.073	5.59	79.22	9.59	119.98	3.55
3	10.387	0.021	0.00000	1.942	0.154	14.74	94.32	9.80	122.48	1.72
4	10.062	0.021	0.00000	0.580	0.193	26.22	98.14	9.88	123.42	1.38
5	10.079	0.021	0.00000	0.822	0.111	32.84	97.43	9.82	122.76	2.36
6	9.931	0.022	0.00000	0.269	0.187	43.95	99.04	9.84	122.95	1.44
7	9.898	0.021	0.01312	0.000	0.257	59.23	99.84	9.88	123.52	0.43
8	9.974	0.022	0.01442	1.352	0.122	66.52	95.85	9.56	119.60	1.99
9	9.895	0.022	0.01297	0.506	0.090	71.88	98.34	9.73	121.67	2.57
10	9.820	0.024	0.03656	0.660	0.096	77.61	97.88	9.61	120.24	2.41
11	9.792	0.021	0.02074	0.690	0.100	83.54	97.77	9.57	119.77	2.36
12	9.824	0.019	0.00000	1.069	0.044	86.17	96.63	9.49	118.79	5.36
13	9.873	0.021	0.00039	1.124	0.118	93.21	96.48	9.53	119.18	2.04
14	9.816	0.021	0.00000	0.723	0.114	100.00	97.66	9.59	119.93	2.19
104-08_am (Fig. 4e)										
1	15.639	0.135	0.10415	36.849	0.041	10.69	30.33	4.74	60.33	9.03
2	12.089	0.202	0.26295	7.452	0.038	20.84	81.82	9.89	123.63	5.91

3	12.980	0.393	0.48942	11.105	0.065	37.92	74.88	9.72	121.57	4.92
4	11.298	0.452	0.51019	5.464	0.059	53.55	85.91	9.71	121.41	4.55
5	10.950	0.501	0.44174	3.405	0.066	70.92	90.97	9.96	124.50	4.06
6	9.795	0.376	0.44907	0.001	0.007	72.73	99.84	9.82	122.70	3.11
7	9.640	0.474	2.81562	0.000	0.037	82.37	99.84	9.85	123.16	1.58
8	9.797	0.283	0.37251	0.000	0.016	86.69	99.84	9.81	122.65	2.07
9	10.080	0.473	0.60058	2.043	0.050	100.00	94.30	9.51	119.00	4.76
<hr/>										
104-08_bt	(Fig. 4e)									
1	10.477	0.106	0.00000	10.719	0.022	1.98	69.62	7.29	91.97	10.62
2	9.725	0.101	0.01153	0.273	0.060	7.29	99.02	9.63	120.45	4.11
3	9.517	0.108	0.15852	0.000	0.023	9.33	99.84	9.51	119.05	1.12
4	9.532	0.105	0.05290	0.000	0.117	19.78	99.84	9.52	119.13	0.60
5	9.560	0.102	0.01769	0.000	0.123	30.71	99.84	9.55	119.44	0.60
6	9.534	0.105	0.00000	0.000	0.045	34.73	99.84	9.52	119.11	0.57
7	9.437	0.101	0.00711	0.000	0.202	52.72	99.83	9.42	117.93	0.62
8	9.487	0.104	0.00000	0.000	0.127	64.03	99.84	9.47	118.54	0.65
9	9.529	0.102	0.01611	0.000	0.118	74.49	99.84	9.51	119.06	0.56
10	9.551	0.102	0.03796	0.000	0.068	80.52	99.84	9.54	119.34	0.60
11	9.613	0.104	0.02359	0.420	0.068	86.56	98.57	9.48	118.59	3.67
12	9.458	0.102	0.00000	0.191	0.151	100.00	99.24	9.39	117.50	1.78

Table 2